At present, however, we do not know what type of MMP is actually responsible for the processing of βDG or if this MMP activity really cleaves the extracellular domain of βDG specifically. In this study, we addressed these issues using the cell culture system of rat schwannoma cell line RT4.

Materials and methods

Cell culture. Rat schwannoma cell line RT4 was described previously [6,7]. RT4 cells were grown in Dulbecco's modified Eagle's medium containing 10% fetal calf serum, 16.7 mM glucose, 2 mM glutamine, 100 U/ml penicillin G sodium, and 100 μg/ml streptomycin. Culture medium was changed every 3 days. When cells grew to near confluence, they were digested with 0.25% trypsin/0.02% EDTA and planted in 10 cm^2 plate at a density (3×10^6/dish) for 3 days in the culture medium without serum and antibiotics. Living cells were harvested by scraping the culture dishes with rubber policemen and homogenized in a buffer containing 50 mM Tris–HCl, pH 7.4, 150 mM NaCl, 0.6 μg/ml pepstatin A, 0.5 μg/ml aprotinin, 0.5 μg/ml leupeptin, 0.75 mM benzamidine, and 0.1 mM PMSF, while the culture medium was gathered and concentrated 20-fold so that the final volume equals that of the total cell homogenate.

Proteolysis of fusion proteins. Glutathione *S*-transferase (GST) fusion proteins of βDG, αDG, and dystrophin were prepared as described previously (Fig. 1) [14]. βDG fusion proteins corresponding to amino acids 654–750 (βDGext) and 775–895 (βDGint) correspond to the entire extracellular and intracellular domains of βDG, respectively (Fig. 1a). αDG fusion proteins corresponding to amino acids 30–341 (αDG N-ter) and 343–652 (αDG C-ter) correspond to the N- and C-terminal domains of αDG, respectively (Fig. 1a). Dys corresponds to amino acids 3054–3271 of dystrophin. Forty nanograms/microliter of fusion proteins were incubated at 37 °C with the RT4 cell homogenate or concentrated cell culture medium. In addition, βDGext was incubated at 37 °C with the concentrated RT4 cell culture medium in the presence or absence of various inhibitors of MMPs. These included (2R)-[(4-biphenylylsulfonyl)amino]-*N*-hydroxy-3-phenylpropionamide (Merck Biosciences), doxycycline hydrochloride (Calbiochem), Ac-Arg-Cys-Gly-Val-Pro-Asp-NH_2 (Calbiochem), and CL-82198 (Calbiochem), which are commercially available inhibitors of MMP-2/MMP-9, MMP-1/MMP-8, MMP-3, and MMP-13, respectively [15–18]. Forty nanograms/microliter of βDGext was also incubated with 2 ng/μl of active human MMP-2 and recombinant human MMP-9 (Calbiochem) at 37 °C. Samples were analyzed by SDS–PAGE and immunoblotting using anti-GST-HRP conjugate (Amersham Biosciences). Molecular mass standards were obtained from BIO-RAD (precision plus protein standards).

Zymography. Zymography of RT4 cell homogenate and culture medium were performed according to von Moers et al. [19]. RT4 cells were harvested and homogenized in 1% SDS, while the cell culture medium was gathered and concentrated to the same volume as the cell homogenate. Samples as well as 1 ng of active human MMP-2 and recombinant human MMP-9 were loaded on a 10% SDS–polyacrylamide gel containing 1 mg/ml gelatin. Electrophoresis was carried out at 100 V for 2.5 h. The gel was then washed twice for 10 min and once for 1 h with 2.5% Triton X-100, 50 mM Tris–HCl, pH 7.5 at 20 °C, to remove SDS and to re-nature the gelatinases. For activation of the enzymes, the gel was incubated in 5 mM $CaCl_2$, 50 mM Tris–HCl, pH 7.5, for 18 h at 37 °C under continuous shaking. After fixation in 40% methanol, 10% acetic acid for 30 min at 20 °C, the gel was stained with 0.5% Coomassie brilliant blue G-250 for 1 h, rinsed in distilled water for 2 h, and destained in 7% acetic acid.

Reverse transcription-polymerase chain reaction (RT-PCR). Total RNA was extracted from RT4 cells using Isogen reagent (Wako). First strand cDNA was synthesized using SuperScript™ III kit (Invitrogen), and served as a template for RT-PCR. Primers used to amplify MMP-2 and MMP-9 were as follows: MMP-2, forward, 5′-GACCTTGACCAGAACACCATCG-3′, reverse, 5′-GCTGTATTCCCGACCGTTGAAC-3′; MMP-9, forward, 5′-CCCCACTTACTTTGGAAACGC-3′, reverse, 5′-AGCCACGACCATACAGATGCTG-3′. PCR products were analyzed on a 2% agarose gel, sub-cloned into the T vector and sequenced using the Thermo Sequenase fluorescent labeled primer cycle sequencing kit (Amersham Pharmacia) on the DSQ-1000L DNA sequencer (Shimazu).

Results

Degradation of the extracellular domain of βDG by the concentrated RT4 cell culture medium

We have reported previously that the putative MMP activity that processes βDG is expressed in RT4 cells [6].

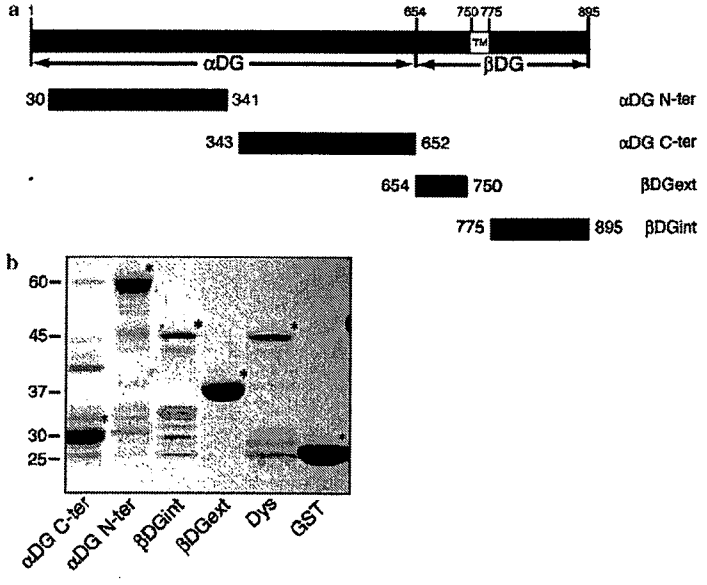

Fig. 1. DG fusion protein constructs. (a) Shown are the fusion protein constructs of DG. TM indicates the single transmembrane domain of βDG. (b) GST fusion proteins were separated by SDS–PAGE and stained with Coomassie brilliant blue. GST fusion proteins corresponding to αDG C-ter, αDG N-ter, βDGint, βDGext, Dys, and GST are indicated by asterisks. Molecular mass standards (Da × 10^3) are shown on the left.

To determine if this protease activity degrades the extracellular or intracellular domain of βDG, we prepared the fusion proteins corresponding to the extracellular domain (βDGext) and intracellular domain (βDGint) of βDG. We incubated βDGext and βDGint with the total RT4 cell homogenate as well as the RT4 cell culture medium concentrated to the same volume as the total cell homogenate. When βDGext was incubated with the cell homogenate or culture medium, it was degraded progressively (Fig. 2a). However, the degradation of βDGext was more prominent with the cell culture medium than cell homogenate (Fig. 2a). These results indicate that the protease activity that degrades βDGext is more abundant in the cell culture medium than cells themselves. On the other hand, βDGint was not degraded at all, when it was incubated with either the RT4 cell homogenate or the concentrated culture medium (Fig. 2b). To further confirm the specificity of degradation of the extracellular domain of βDG, we prepared various fusion proteins, including αDG N-ter, αDG C-ter, Dys, and GST. None of them were degraded, when they were incubated with either the RT4 cell homogenate or the concentrated culture medium (Fig. 2b). Altogether, these results indicate that the RT4 cell culture medium is enriched with the protease activity that degrades the extracellular domain of βDG specifically.

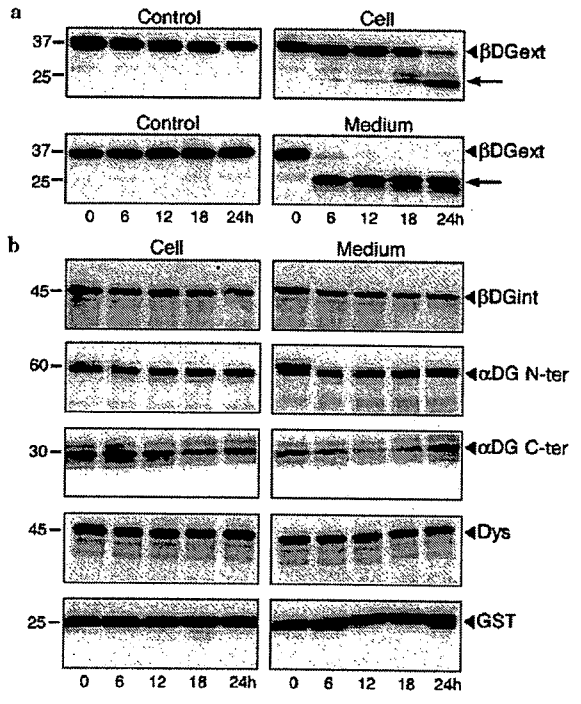

Fig. 2. Specific degradation of βDGext by RT4 cell homogenate and culture medium. (a) βDGext was incubated with the total RT4 cell homogenate as well as the RT4 cell culture medium concentrated to the same volume as the total cell homogenate for various time periods, and analyzed by immunoblotting using anti-GST-HRP conjugate. For controls, βDGext was incubated with the cell homogenization buffer and the concentrated control medium, respectively. The bands indicated by arrows are presumed degradation products of βDGext, because they were detected by anti-GST-HRP conjugate. (b) βDGint, αDG N-ter, αDG C-ter, Dys, and GST were incubated with the RT4 cell homogenate and culture medium for various time periods, and analyzed by immunoblotting using anti-GST-HRP conjugate. Molecular mass standards (Da × 10^3) are shown on the left.

Effects of MMP inhibitors on the degradation of βDGext by the concentrated RT4 cell culture medium

To see if MMPs are involved in the degradation of βDGext, we incubated βDGext with the concentrated RT4 cell culture medium in the presence or absence of inhibitors of MMP-2/MMP-9, MMP-1/MMP-8, MMP-3, and MMP-13 [15–18]. The degradation of βDGext was significantly reduced only by the inhibitor of MMP-2/MMP-9, but not by the inhibitor of MMP-1/MMP-8, MMP-3 or MMP-13 (Fig. 3).

Expression of MMP-2 and MMP-9 in RT4 cells and cell culture medium

To see if MMP-2 and MMP-9 are expressed in RT4 cells and cell culture medium, we performed zymographic analysis of MMP-2 and MMP-9. The 66 kDa band of activated MMP-2 and the 83 kDa band of activated MMP-9 were

Fig. 3. Effects of MMP inhibitors on the degradation of βDGext. βDGext was incubated with the concentrated RT4 cell culture medium in the absence or presence of inhibitors of various MMPs and analyzed by immunoblotting using anti-GST-HRP conjugate. The bands indicated by arrows are presumed degradation products of βDGext, because they were detected by anti-GST-HRP conjugate. Molecular mass standards (Da × 10^3) are shown on the left.

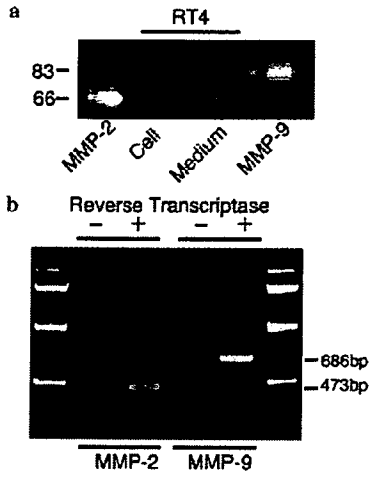

Fig. 4. Expression of MMP-2 and MMP-9 in RT4 cells and RT4 cell culture medium. (a) Zymography of RT4 cells and RT4 cell culture medium. RT4 cell homogenate and culture medium, as well as active human MMP-2 and recombinant human MMP-9, were applied for zymography. Molecular mass standards (Da × 10^3) are shown on the left. (b) RT-PCR analysis of the total RNA from RT4 cells. mRNAs for MMP-2 and MMP-9 were amplified in the presence or absence of reverse transcriptase.

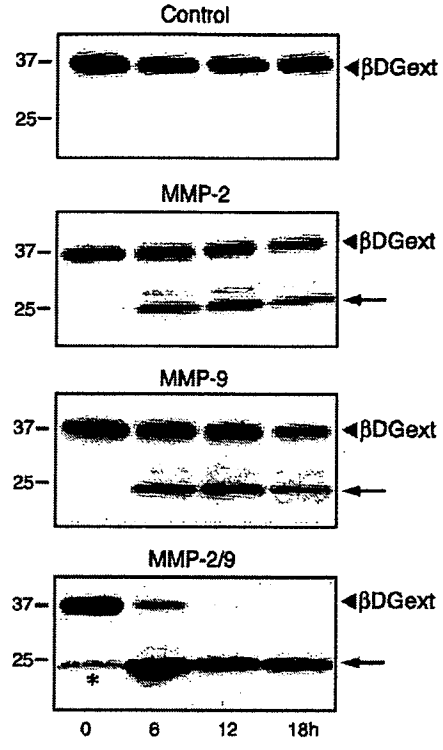

Fig. 5. Degradation of βDGext by active MMP-2 and MMP-9 enzymes. Forty nanograms/microliter of βDGext was incubated with 2 ng/μl of active human MMP-2 and recombinant human MMP-9 for various time periods. Samples were analyzed by immunoblotting using anti-GST-HRP conjugate. The bands indicated by arrows are presumed degradation products of βDGext, because they were detected by anti-GST-HRP conjugate. The band indicated by the asterisk in the lane of 0 h is an overflow from the lane of 6 h. Molecular mass standards (Da × 10^3) are shown on the left.

detected in the RT4 cell culture medium, while they were not detected in the total RT4 cell homogenate (Fig. 4a). We performed RT-PCR analysis of the total RNA from RT4 cells. A single PCR fragment of the expected size was detected for both MMP-2 and MMP-9 (Fig. 4b). We excised and subcloned the PCR products and confirmed that the products had the sequence of rat MMP-2 and MMP-9 (data not shown). These results indicate the de novo synthesis of MMP-2 and MMP-9 in RT4 cells and their secretion into the culture medium.

Degradation of βDGext by MMP-2 and MMP-9

To see if MMP-2 and MMP-9 are involved in the processing of βDG, we incubated βDGext with the active enzymes of MMP-2 and MMP-9. βDGext was degraded progressively by the incubation with either MMP-2 or MMP-9 (Fig. 5). Moreover, the degradation of βDGext was augmented significantly when it was incubated with both MMP-2 and MMP-9 (Fig. 5).

Discussion

In this study, we found that the culture medium of RT4 cells was enriched with the protease activity that degrades the fusion protein construct of the extracellular domain of βDG specifically. This activity was suppressed by the inhibitor of MMP-2 and MMP-9, but not by the inhibitors of MMP-1, MMP-3, MMP-8, and MMP-13. Zymography and RT-PCR analysis showed that RT4 cells secreted MMP-2 and MMP-9 into the culture medium. Finally, active MMP-2 and MMP-9 enzymes degraded the fusion protein construct of the extracellular domain of βDG. These results indicate (1) that RT4 cells secrete the protease activity that degrades the extracellular domain of βDG specifically and (2) that MMP-2 and MMP-9 may be involved in this process.

Disruption of the link between the ECM and cell membrane via the DG complex is presumed to have a deleterious effect on the stability of cell membrane and viability of cells [6]. MMPs are the candidate molecules that degrade the components of the DG complex and disrupt this link [6–13]. In this context, it is noteworthy that MMPs have been implicated in the molecular pathogenesis of muscular dystrophies. von Moers et al. reported that gelatinolytic activity of MMP-2 was increased in the skeletal muscle of DMD [19]. Kherif et al. reported that both pro and active forms of MMP-2 and MMP-9 were expressed in the skeletal muscle of *mdx* mice [20]. Lattanzi et al. reported the aberrantly processed laminin α2 chain and increased activity of MMP-2/MMP-14 in the cultured skeletal muscle cells of congenital muscular dystrophy [21]. Interestingly, it has recently been reported that the processing of DG by MMP-2 and MMP-9 may be involved in the leukocyte extravasation in experimental autoimmune encephalomyelitis [22].

The present study, which demonstrates the secretion of the protease activity that degrades the extracellular domain of βDG by cultured cells and points to the roles of MMP-2 and MMP-9 in this process, would further help to broaden our understanding of the complex mechanisms involved in the processing of βDG.

Acknowledgments

We thank Miki Yamanaka and Yuka Sasayama for their expert technical assistance. This work was supported by [1] Research Grants 16B-1 and 17A-10 for Nervous and Mental Disorders (Ministry of Health, Labor and Welfare), [2] Research on Psychiatric and Neurological Diseases and Mental Health (Ministry of Health, Labor and Welfare), and [3] Research Grants 16390256, 40286993, and "Open Research Center" Project for Private Universities: matching fund subsidy from MEXT (Ministry of Education, Culture, Sports, Science, and Technology), 2004–2008.

References

[1] O. Ibraghimov-Beskrovnaya, J.M. Ervasti, C.J. Leveille, C.A. Slaughter, S.W. Sernett, K.P. Campbell, Primary structure of dystrophin-associated glycoproteins linking dystrophin to the extracellular matrix, Nature 355 (1992) 696–702.

[2] M.D. Henry, K.P. Campbell, Dystroglycan: an extracellular matrix receptor linked to the cytoskeleton, Curr. Opin. Cell Biol. 8 (1996) 625–631.

[3] J.M. Ervasti, K.P. Campbell, Membrane organization of the dystrophin-glycoprotein complex, Cell 66 (1991) 1121–1131.

[4] A. Suzuki, M. Yoshida, K. Hayashi, Y. Mizuno, Y. Hagiwara, E. Ozawa, Molecular organization at the glycoprotein-complex-binding-site of dystrophin. Three dystrophin-associated proteins bind directly to the carboxy-terminal portion of dystrophin, Eur. J. Biochem. 220 (1994) 283–292.

[5] E. Di Stasio, F. Sciandra, B. Maras, F. Di Tommaso, T.C. Petrucci, B. Giardina, A. Brancaccio, Structural and functional analysis of the N-terminal extracellular region of β-dystroglycan, Biochem. Biophys. Res. Commun. 206 (1999) 274–278.

[6] H. Yamada, F. Saito, H. Fukuta-Ohi, D. Zhong, A. Hase, K. Arai, A. Okuyama, R. Maekawa, T. Shimizu, K. Matsumura, Processing of β-dystroglycan by matrix metalloproteinase disrupts the link between the extracellular matrix and cell membrane via the dystroglycan complex, Hum. Mol. Genet. 15 (2001) 1563–1569.

[7] K. Matsumura, K. Arai, D. Zhong, F. Saito, H. Fukuta-Ohi, R. Maekawa, H. Yamada, T. Shimizu, Disruption of dystroglycan axis by β-dystroglycan processing in cardiomyopathic hamster muscle, Neuromuscul. Disord. 13 (2003) 796–803.

[8] K. Matsumura, D. Zhong, F. Saito, K. Arai, K. Adachi, H. Kawai, I. Higuchi, I. Nishino, T. Shimizu, Proteolysis of β-dystroglycan in muscular diseases, Neuromuscul. Disord. 15 (2005) 336–341.

[9] C. Herzog, C. Has, C.W. Franzke, F.G. Echtermeyer, U. Schlotzer-Schrehardt, S. Kroger, E. Gustafsson, R. Fassler, L. Bruckner-Tuderman, Dystroglycan in skin and cutaneous cells: β-subunit is shed from the cell surface, J. Invest. Dermatol. 122 (2004) 1372–1380.

[10] C. Losasso, F. Di Tommaso, A. Sgambato, R. Ardito, A. Cittadini, B. Giardina, T.C. Petrucci, A. Brancaccio, Anomalous dystroglycan in carcinoma cell lines, FEBS Lett. 484 (2000) 194–198.

[11] A. Sgambato, M. Migaldi, M. Montanari, A. Camerini, A. Brancaccio, G. Rossi, R. Cangiano, C. Losasso, G. Capelli, G.P. Trentini, A. Cittadini, Dystroglycan expression is frequently reduced in human breast and colon cancers and is associated with tumor progression, Am. J. Pathol. 162 (2003) 849–860.

[12] J. Jing, C.F. Lien, S. Sharma, J. Rice, P.A. Brennan, D.C. Gorecki, Aberrant expression, processing and degradation of dystroglycan in squamous cell carcinomas, Eur. J. Cancer 40 (2004) 2143–2151.

[13] L. Leone, M.E. De Stefano, A. Del Signore, T.C. Petrucci, P. Paggi, Axotomy of sympathetic neurons activates the metalloproteinase-2 enzymatic pathway, J. Neuropathol. Exp. Neurol. 64 (2005) 1007–1017.

[14] F. Saito, T. Masaki, K. Kamakura, L.V.B. Anderson, S. Fujita, H. Fukuta-Ohi, Y. Sunada, T. Shimizu, K. Matsumura, Characterization of the transmembrane molecular architecture of the dystroglycan complex in schwann cells, J. Biol. Chem. 274 (1999) 8240–8246.

[15] Y. Tamura, F. Watanabe, T. Nakatani, K. Yasui, M. Fuji, T. Komurasaki, H. Tsuzuki, R. Maekawa, T. Yoshioka, K. Kawada, K. Sugita, M. Ohtani, Highly selective and orally active inhibitors of type IV collagenase (MMP-9 and MMP-2): *N*-sulfonylamino acid derivatives, J. Med. Chem. 41 (1998) 640–649.

[16] R. Hanemaaijer, T. Sorsa, Y.T. Konttinen, Y. Ding, M. Sutinen, H. Visser, V.W. van Hinsbergh, T. Helaakoski, T. Kainulainen, H. Ronka, H. Tschesche, T. Salo, Matrix metalloproteinase-8 is expressed in rheumatoid synovial fibroblasts and endothelial cells. Regulation by tumor necrosis factor-α and doxycycline, J. Biol. Chem. 272 (1997) 31504–31509.

[17] N. Fotouhi, A. Lugo, M. Visnick, L. Lusch, R. Walsky, J.W. Coffey, A.C. Hanglow, Potent peptide inhibitors of stromelysin based on the prodomain region of matrix metalloproteinases, J. Biol. Chem. 269 (1994) 30227–30231.

[18] J.M. Chen, F.C. Nelson, J.I. Levin, D. Mobilio, F.J. Moy, R. Nilakantan, A. Zask, R. Powers, Structure-based design of a novel, potent, and selective inhibitor for MMP-13 utilizing NMR spectroscopy and computer-aided molecular design, J. Am. Chem. Soc. 122 (2000) 9648–9654.

[19] A. von Moers, A. Zwirner, A. Reinhold, O. Bruckmann, F. van Landeghem, G. Stoltenburg-Didinger, D. Schuppan, H. Herbst, M. Schuelke, Increased mRNA expression of tissue inhibitors of metalloproteinase-1 and -2 in Duchenne muscular dystrophy, Acta Neuropathol. 109 (2005) 193–285.

[20] S. Kherif, C. Lafuma, M. Dehaupas, S. Lachkar, J.G. Fournier, M. Verdiere-Sahuque, M. Fardeau, H.S. Alameddine, Expression of matrix metalloproteinases 2 and 9 in regenerating skeletal muscle: a study in experimentally injured and mdx muscles, Dev. Biol. 205 (1999) 158–170.

[21] G. Lattanzi, F. Muntoni, P. Sabatelli, S. Squarzoni, N.M. Maraldi, V. Cenni, M. Villanova, M. Columbaro, L. Merlini, S. Marmiroli, Unusual laminin α2 processing in myoblasts from a patient with a novel variant of congenital muscular dystrophy, Biochem. Biophys. Res. Comm. 277 (2000) 639–642.

[22] S. Agrawal, P. Anderson, M. Durbeej, N. van Rooijen, F. Ivars, G. Opdenakker, L.M. Sorokin, Dystroglycan is selectively cleaved at the parenchymal basement membrane at sites of leukocyte extravasation in experimental autoimmune encephalomyelitis, J. Exp. Med. (2006), Epub ahead of print.

PERGAMON

Neuromuscular Disorders 17 (2007) 306–312

www.elsevier.com/locate/nmd

Expression of MBNL and CELF mRNA transcripts in muscles with myotonic dystrophy

Yuriko Nezu [a], Yoshihiro Kino [b], Noboru Sasagawa [a], Ichizo Nishino [c], Shoichi Ishiura [a,*]

[a] *Department of Life Sciences, Graduate School of Arts and Sciences, The University of Tokyo, Tokyo, Japan*
[b] *Laboratory for Structural Neuropathology, RIKEN Brain Science Institute, Wako-shi, Saitama, Japan*
[c] *National Institute of Neuroscience, NCNP, Kodaira, Tokyo, Japan*

Received 29 September 2006; received in revised form 24 December 2006; accepted 8 January 2007

Abstract

Myotonic dystrophy type 1 (DM1) is an autosomal dominant disorder that causes muscle wasting, myotonia, cardiac conduction abnormalities, and other multi-systemic symptoms. Current evidence supports a pathogenic mechanism involving aberrantly expanded CTG repeats in the 3′-untranslated region of the DM-protein kinase (*DMPK*) gene. The repeats are thought to recruit various RNA-binding proteins such as muscleblind-like (MBNL) proteins into foci in the nuclei of DM cells, resulting in loss of function. However, aberrant regulation of transcription or subsequent RNA processing of MBNL-family mRNAs might also be part of the pathogenic mechanism of DM. We used real-time RT-PCR analysis to examine the possibility that MBNL mRNA expression is altered in DM1 patients. We also examined mRNA expression for members of the CUG-BP and ETR-3-like factor (CELF) family of RNA-binding proteins given that CELF proteins regulate alternative splicing and are also implicated in DM. We found that DM1 muscles displayed aberrant regulation of alternative splicing as reported previously; however, the levels of MBNL and CELF mRNA expression did not show any significant changes. Our results suggest that the expression and stability of the mRNA for these RNA-binding proteins are unaffected in DM1.

Keywords: Alternative splicing; CUG-BP- and ETR-3-like family; Muscleblind; Myotonic dystrophy

1. Introduction

Myotonic dystrophy (DM) is an autosomal dominant disorder and the most common form of muscular dystrophy affecting adults [1]. Multiple systems are affected in DM patients, and characteristic symptoms include muscle hyperexcitability (myotonia), cataracts, defects in cardiac conduction, mental retardation, and insulin resistance [1].

Two forms of DM have been identified thus far, DM1 and DM2. The gene affected in DM1 is *DM protein kinase* (*DMPK*) on chromosome 19q. This gene contains CTG trinucleotide repeats within its 3′-untranslated region (UTR) [2,3]. The expansion of this repeat has been known to trigger the pathogenesis of DM1 and interestingly, the number of repeats is thought to be correlated with symptom severity [3].

The gene affected in DM2 is *zinc-finger protein 9* (*ZNF9*). This gene contains CCTG tetranucleotide repeats in intron 1, and as in DM1, expansion of this repeat is believed to be the cause of this disease [4]. The most strongly supported pathogenic hallmark is that the expanded repeat-containing mRNA transcribed from the altered *DMPK* and *ZNF9* genes forms foci that are retained within the nuclei of DM cells [4–6]. Given that DM1 and DM2 have phenotypic overlap in spite

* Corresponding author. Tel.: +81 5454 6739.
E-mail address: cishiura@mail.ecc.u-tokyo.ac.jp (S. Ishiura).

0960-8966/$ - see front matter © 2007 Elsevier B.V. All rights reserved.
doi:10.1016/j.nmd.2007.01.002

of the different loci of *DMPK* and *ZNF9*, this finding suggests that the expanded repeats themselves cause DM. Indeed, transgenic mice expressing human skeletal actin containing expanded CUG repeats manifest some DM symptoms, including myotonia [6].

The nuclear foci found in DM cells appear to recruit certain RNA-binding proteins, thus disrupting the proper functions of these proteins (loss of function) [7,8]. One family of RNA-binding proteins thus affected is the muscleblind (MBNL) family, consisting of MBNL1, MBNL2, and MBNL3 in humans [8]. Each of these proteins has been shown to co-localize with RNA foci in both DM1 and DM2 cells [8]. The MBNL proteins are zinc-finger proteins that bind to both CUG and CCUG repeats [9,10], and act as regulators of alternative splicing of certain genes that are strongly implicated in some of the symptoms of DM1. In particular, the myotonia and insulin resistance of DM1 are caused by defects in chloride channel and insulin receptor (IR) proteins, respectively, that arise because the MBNL protein is trapped in the nuclear foci and thus suffers loss of function [11–13]. Importantly, MBNL1-knockout mice exhibit some DM symptoms such as myotonia and cataracts [11], which strongly supports the involvement of MBNL proteins in the pathogenesis of DM1.

Another group of proteins strongly implicated in DM pathogenesis is the CUG-BP and ETR-3-like factor (CELF) family, which regulates alternative splicing [14–19], translation [20,21], and deadenylation [22]. Upregulation of CUG-BP protein expression has been implicated in the DM1 mechanism [14,23], suggesting that abnormal activation of CUG-BP might be involved in DM1 pathogenesis. In addition, some studies have suggested a strong involvement of CELF in DM pathogenesis, indicating that CUG-BP transgenic mice exhibit DM-like symptoms [23,24]. CUG-BP and other CELF members can regulate alternative splicing of various pre-mRNAs that are important in DM1 pathogenesis, including pre-mRNAs for IR and cardiac troponin T (cTNT) [16,24–28].

Loss of function of MBNL proteins [11,13] and altered activity [23,24,29] or localization of CELF proteins [30] have been suggested as possible pathogenic mechanisms in DM. However, aberrant regulation of transcription or subsequent RNA processing of MBNL- and CELF-family mRNAs might also be part of the DM mechanism. To our knowledge, however, this has not been previously addressed.

The functions of non-coding RNA have been the subject of increased attention. These functions include roles in DNA replication, chromosome maintenance, and regulation of transcription, as well as RNA processing, translation, and mRNA stability. One study reported that expanded CUG repeats in *DMPK* tend to form a double-helical RNA hairpin, which could be a source of microRNA and/or small interfering RNA. It also noted that MBNL contains a sequence that is almost complementary to the CUG repeats of *DMPK* [31]. These findings suggest that the CUG repeats in *DMPK* mRNA may silence expression of MBNL1, although this mechanism has not been confirmed experimentally.

In the present study, we examined whether altered expression of MBNL and CELF proteins has any relevance for understanding DM pathogenesis. Using RT-PCR, we compared the expression of MBNL and CELF mRNA in DM1 patients and non-DM individuals to determine whether expression is indeed altered in DM1.

2. Materials and methods

2.1. Tissue samples

Biopsy materials were obtained from the biceps (brachii muscle) or quadriceps (femoris muscle) of 20 DM1 patients (11 males and 9 females, 11–68 years old) and 12 confirmed non-DM individuals with no histological abnormality. All samples were stored at −80 °C. Clinically, all DM1 samples had muscle weakness with myotonia. Myotonic discharge that was detectable by EMG. Onset was during childhood or adolescence except for a 21-year-old patient who had congenital onset. Pathologically, all DM1 samples showed myopathic change with variation in fiber size. Some displayed fibers with internalized nuclei (>5%; 16/20 patients, 90%), type 1 fiber predominance (10/20, 50%), endomysial fibrosis (16/20, 80%), adipose tissue replacement (6/20, 30%), sarcoplasmic mass (7/20, 35%), and pyknotic nuclear clumps (17/20, 85%). Relatively extensive fibrosis was seen in three patients and mild adipose tissue replacement in two.

All biopsy materials used in this study were acquired with informed consent.

2.2. Real-time RT-PCR

Total RNA was isolated from the biopsy samples using Concert™ Cytoplasmic RNA Reagent (Invitrogen, Carlsbad, CA), treated with DNase, and purified by standard phenol–chloroform extraction and isopropanol precipitation. cDNA synthesis was performed using a template consisting of 100 ng total RNA and the ThermoScript™ RT-PCR System (Invitrogen) with a mixture of oligo$(dT)_{20}$ and random hexamers on a 10-μl scale. The cDNA was then diluted 50-fold with sterile water, and 10 μl of diluted cDNA was used for the real-time RT-PCR measurements.

All primers used for generation of a standard curve template and for the quantification of IR-A, IR-B, GAPDH, β-actin, HPRT, MBNL and CELF mRNAs were designed using Primer 3 software (Whitehead Institute for Biomedical Research, Totowa, NJ). The primer sequences (shown $5' \rightarrow 3'$) were as follows. IR-A:

TGCTG CTCCT GTCCA AAGAC and GAGAT GGACT GGGGA CGAAA; IR-B: TTCGT CCCCA GAAAA ACCTC and CACCG TCACA TTCCC AACAT; GAPDH: GAGTC AACGG ATTTG GTCGT and AATGA AGGGG TCATT GATGG; β-actin: GACAG GATGC AGAAG GAGAT TACT and TGATC CACAT CTGCT GGAAG GT; HPRT: TGAGG ATTTG GAAAG GGTGT and CATCT CGAGC AAGAC GTTCA; MBNL1: GGGTT TGTTG GTTTC ACTG and TGTCC CGAAT TGGTG TGA; MBNL2: CCACC ACGCC TGTTA TTGTT and CCCTG CATAC CTCCA GTTTG; CUG-BP: CTGGA AGCCA GAAGG AAGGT and GCAGG TCCTG ATCAC CAAAC; ETR-3: CAGGG TGATG TTCTC TCCAT TT and GCCTC GACTC AGCCC ATC.

Total RNA from skeletal muscle (BD Biosciences, Franklin Lakes, NJ) was reverse-transcribed to synthesize the cDNA, which was then used as the template for the standards. Three housekeeping genes were chosen as calibration standards: β-actin, HPRT, and GAPDH.

cDNA calibrators were prepared by PCR amplification of HEK293 cell cDNA with the primers listed above. The resulting PCR products yielded unique bands by agarose gel electrophoresis and were purified by gel extraction using GeneEluteTM Agarose Spin Columns (Sigma, St. Louis, MO) followed by standard phenol–chloroform extraction. The concentrations of these calibrators were determined using a spectrophotometer (NanoDrop Technologies, Wilmington, DE). Concentrations were calibrated from 1.0×10^{-5} to 1.0×10^{-9} μg/μl by serial 10-fold dilutions. The PCR products above were cloned into pGEM®-T-Easy vector (Promega, Madison, WI) and their sequences were confirmed with the CEQTM 8000 Genetic Analysis System (Beckman Coulter, Fullerton, CA).

Real-time PCR was performed on a 7300 Real-Time PCR System (Applied Biosystems, Foster City, CA) using SYBR Premix Ex Taq™ (TaKaRa Bio, Tokyo, Japan). The thermal profile consisted of an initial incubation at 95 °C for 10 s followed by 40 cycles at 95 °C for 5 s and 60 °C for 34 s. To assure specific amplification, dissociation temperatures were measured after each run. The 7300 Real-Time PCR System software was used to determine the crossing points for the individual samples, including those for the calibration standards. The expression levels of the target genes were normalized relative to expression of the β-actin gene.

For each run, data acquisition and analysis was performed using the 7300 Real-Time PCR System software. As all samples were available only in a limited amount, the mean values and *p*-values were determined by Student's *t*-test, but not the variance.

2.3. Splicing assays

cDNAs produced as described above were used as templates for the RNA splicing assay. PCR was performed using the primers and thermal conditions described below. For the cTNT splicing assay, the forward and reverse primers (shown 5′ → 3′) were ATAGA AGAGG TGGTG GAAGA GTAC and GTCTC AGCCT CTGCT TCAGC ATCC, respectively; 35 cycles of amplification were performed, each consisting of 30 s at 96 °C, 30 s at 63 °C, and 30 s at 72 °C, followed by a final 5 min extension at 72 °C. For the IR splicing assay, the forward and reverse primers were CCAAA GACAG ACTCT CAGAT and AACAT CGCCA AGGGA CCTGC, respectively; 35 cycles of amplification were performed, each consisting of 30 s at 96 °C, 30 s at 60 °C, and 30 s at 72 °C, followed by a final 5 min extension at 72 °C. The PCR products were resolved on a 10% polyacrylamide gel that was stained with ethidium bromide and analyzed using an LAS-3000 luminescence image analyzer (Fujifilm, Tokyo, Japan).

3. Results

3.1. Aberrant splicing in DM1

We used RT-PCR to examine several genes already known to undergo abnormal alternative splicing to determine whether aberrant regulation of alternative splicing was evident in the study samples. Cardiac troponin T (cTNT) is known to shift from an immature isoform to a mature isoform during heart development and it has been reported that cardiac tissues and skeletal muscle from DM1 patients display an inappropriate retention of fetal exon 5 of cTNT [32]. Our RT-PCR analysis using RNA isolated from 20 DM patients and 12 non-DM individuals showed significant promotion of exon 5 inclusion in DM skeletal muscle (Fig. 1a), thus supporting the previous findings. Furthermore, as was also reported previously, inclusion of exon 5 was notably promoted in DM tissues, with a 1.8-fold increase in the average ratio of exon 5 inclusion (Fig. 1b).

Alternative splicing of the 36-nucleotide exon 11 of the insulin receptor (IR) gene yields two isoforms, IR-A (exon 11 removed) and IR-B (exon 11 retained). The IR-B isoform is predominant in the insulin-responsive tissues that are responsible for glucose homeostasis, such as adipose tissues, liver, and skeletal muscle whereas in skeletal muscle from DM1 patients, the IR-A isoform is most common [14]. This switching of IR isoforms has not been observed in other myopathies [14]. We found that retention of IR exon 11 was strongly suppressed in DM1 patients, whereas IR-B was predominant in non-DM individuals. The average ratio of exon 11 retention decreased from 0.56 (non-DM) to 0.26

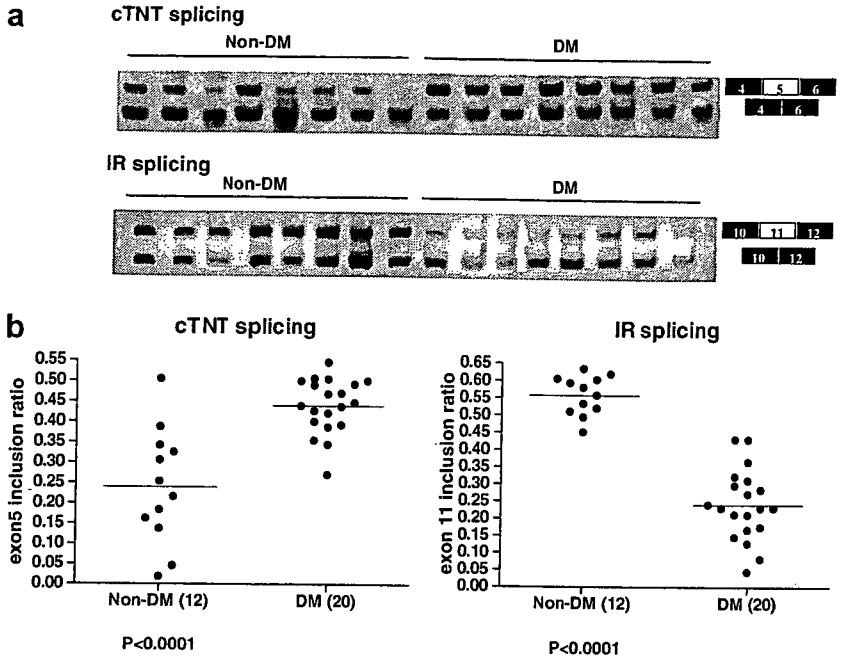

Fig. 1. Alternative splicing of cardiac troponin T (cTNT) and insulin receptor (IR) RNA. (a) Splicing products obtained by RT-PCR amplification of RNA isolated from non-DM control ($n = 8$) and DM1 ($n = 8$) biopsy samples. The exon utilization for each splicing product is shown. (b) Quantification of the RT-PCR products was performed among 20 DM1 samples and 12 non-DM individuals by using LAS-3000 luminescence image analyzer (Fujifilm). The graphs show the ratio of the alternative exon inclusion of cTNT and IR.

(DM; Fig. 1b). Therefore, the biopsy tissues used in this study manifested aberrant regulation of alternative splicing – a characteristic feature of DM pathogenesis.

3.2. Expression of mRNAs for MBNL1, MBNL2, CUG-BP, and ETR-3

An important consideration in interpreting the observed changes in splicing patterns is that both MBNL loss of function and CELF activation could explain our results [12]. For example, the retention of cTNT exon 5 is promoted by CELF but repressed by MBNL proteins. Conversely, the retention of IR exon 11 is promoted by MBNL but repressed by CELF proteins. Therefore, we sought to determine whether the observed altered splicing patterns resulted from loss of MBNL function and/or activation of CELF function.

To determine the degree of change detectable by this method, we measured the expression of insulin receptor isoform B (IR-B), which has been shown by gel electrophoresis to be downregulated in DM patients (Fig. 1). The results indicated that, as predicted, the DM patients expressed significantly less IR-B compared to the non-DM group (Fig. 2a). However, nine DM samples (out of 20) showed particularly high levels of downregulation such that their expression levels did not reach the range in which the accuracy of this method is assured by the standard curve. However, when these data were omitted from the analysis, this quantification method still successfully showed a 2- to 3-fold difference in expression levels, thus testifying to the suitability of this method for our experiment. Expression of IR-A was also measured and no significant differences were observed between non-DM and DM patients (Fig. 2a), as was expected from the results shown in Fig. 1.

We also performed real-time PCR analysis to measure the expression of MBNL and CELF mRNA. Total RNA was extracted from 20 DM and 12 non-DM biopsy samples, and the RNA was reverse-transcribed using a mixture of oligo(dT) and random hexamers. To allow for rigorous calibration of the data, we also examined mRNA expression for three commonly used housekeeping proteins, β-actin, GAPDH, and hypoxanthine–guanine phosphoribosyl transferase (HPRT). Comparing the relative mRNA level of each protein to that of the other two mRNAs allowed us to identify the gene with the most stable expression. We found that while the HPRT/GAPDH and β-actin/GAPDH ratios exhibited significant variation, the HPRT/β-actin ratio remained relatively constant among all smples. This indicated that HPRT and β-actin were reliable housekeeping genes; therefore, we selected the β-actin gene for normalization of the real-time PCR data.

We found no significant differences between DM and non-DM individuals with respect to mRNA levels for MBNL1, MBNL2, CUG-BP, and ETR-3 using real-time PCR (Fig. 2b), suggesting that the expression or stability of these mRNAs is not affected in DM. However, as shown in Fig. 2b, substantial individual variation

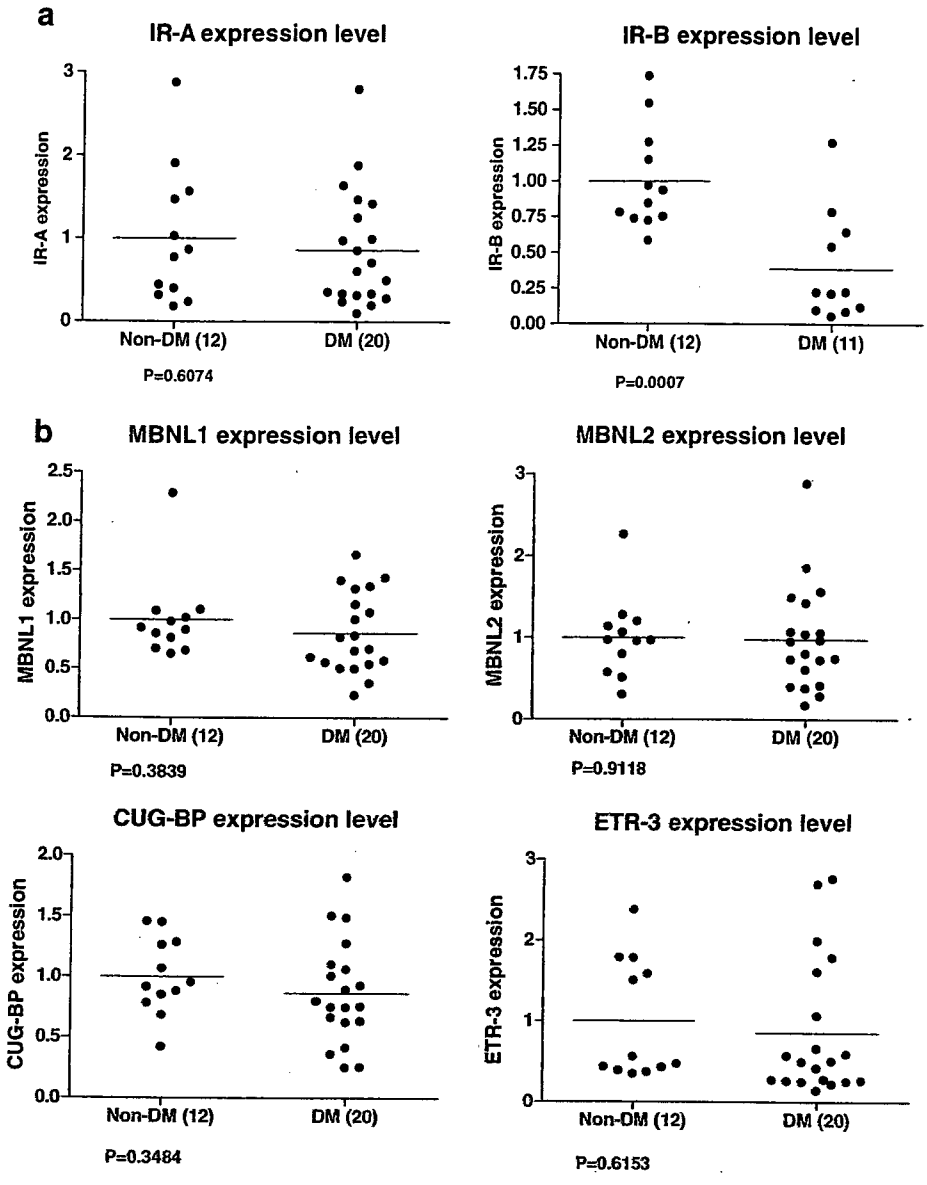

Fig. 2. (a) Expression of isoform A and B of insulin receptor in DM and non-DM samples determined by Real-time PCR. (b) Real-time RT-PCR analysis of relative expression levels of MBNL1, MBNL2, CUG-BP, and ETR-3 mRNAs in 21 DM-patients and 12 non-DM individuals. All data were normalized relative to β-actin mRNA expression. The values shown in the graphs have been divided by the average value for non-DM individuals.

in levels of these mRNAs was observed. We had predicted that the CELF and MBNL mRNA levels would be correlated with the extent of altered splicing seen in DM patients; however, our results did not support this hypothesis. Instead, DM individuals exhibiting significantly increased retention of cTNT exon 5 did not necessarily display significant abnormalities in IR splicing. Furthermore, mRNA expression of the four RNA-binding proteins examined in this experiment did not result in a significant change in IR splicing (data not shown).

The mRNA expression levels for the remaining MBNL and CELF proteins were so low that quantifying them was technically difficult in both DM and non-DM individuals. Previous reports have also described low expression levels for these proteins in muscles of normal individuals [33,34].

4. Discussion

The objective of this study was to determine whether a difference exists in mRNA expression levels of MBNL and CELF proteins between DM and non-DM muscles. Measurement by real-time RT-PCR showed that mRNA expression levels for these proteins were not significantly altered in DM patients. However, splice variants of MBNL proteins were not distinguished in this experiment because the primers for the real-time PCR assay were designed to amplify a fragment common to

all the known variants. MBNL1 has at least nine variants [10], some of which lack zinc-finger motifs and therefore probably do not interact with mRNA. The relevance of the other variants remains largely unknown. The observation that the MBNL1 isoform with exon 5 retained localizes in nuclei, where alternative splicing takes place, and therefore it has the largest potential (i.e., the most opportunity) to influence alternative splicing is noteworthy (Kino et al., unpublished data). Thus, the abundance ratio of these variants may be altered in DM1, which may influence MBNL1 function in cells.

We also found that levels of CUG-BP and ETR-3 mRNA were not significantly different for DM and non-DM individuals. During heart development, CUG-BP and ETR-3 undergo strong downregulation, whereas MBNL1 and MBNL2 expression is maintained [35]. Our findings suggest that expression of CUG-BP and ETR-3 mRNA is regulated normally throughout muscle development in DM patients. Whether the expression of CUG-BP and ETR-3 is altered at the protein level in DM patients is thus an important question. While increased levels of CUG-BP protein have been observed in DM1 tissues [14,23], this increase could be a result of altered posttranscriptional processing affecting translation, phosphorylation, or proteolytic degradation rather than altered regulation of transcription or mRNA stability.

In summary, our data confirmed the occurrence of aberrant splicing regulation in DM1 patients and demonstrated that these abnormalities are not associated with any altered expression of MBNL or CELF mRNA.

Acknowledgments

This work was supported by research grants from the Ministry of Health, Labor, and Welfare, Japan.

References

[1] Harper PS. Myotonic Dystrophy. 3rd ed. London: WB Sauders; 2001.

[2] Brook JD, McCurrach ME, Harley HG, Buckler AJ, Church D, Aburatani H, et al. Molcular basis of myotonic dystrophy: expansion of a trinucleotide (CTG) repeat at the 3′ end of a transcript encoding a protein kinase family member. Cell 1992;68:799–808.

[3] Mahadevan M, Tsilfidis C, Sabourin L, Shutler G, Amemiya C, Jansen G, et al. Myotonic dystrophy mutation: an unstable CTG repeat in the 3′ untranslated region of the gene. Science 1992;255:1253–5.

[4] Liquori CL, Ricker K, Moseley ML, Jacobsen JF, Kress W, Naylor SL, et al. Myotonic dystrophy type 2 caused by a CCTG expansion in intron 1 of ZNF9. Science 2001;293:864–7.

[5] Taneja KL, McCurrach M, Schalling M, Housman D, Singer RH. Foci of trinucleotide repeat transcripts in nuclei of myotonic dystrophy cells and tissues. J Cell Biol 1995;128: 995–1002.

[6] Mankodi A, Logigian E, Callahan L, McClain C, White R, Henderson D, et al. Myotonic dystrophy in transgenic mice expressing an expanded CUG repeat. Science 2000;289: 1769–73.

[7] Fardaei M, Larkin K, Brook JD, Hamshere MG. In vivo co-localisation of MBNL protein with DMPK expanded-repeat transcripts. Nucleic Acids Res 2001;29:2766–71.

[8] Fardaei M, Rogers MT, Thorpe HM, Larkin K, Hamshere MG, Harper PS, et al. Three proteins, MBNL, MBLL and MBXL, co-localize in vivo with nuclear foci of expanded-repeat transcripts in DM1 and DM2 cells. Hum Mol Genet 2002;11:805–14.

[9] Miller JW, Urbinati CR, Teng-Umnuay P, Stenberg MG, Byrne BJ, Thornton CA, et al. Recruitment of human muscleblind proteins to (CUG)(n) expansions associated with myotonic dystrophy. EMBO J 2000;19:4439–48.

[10] Kino Y, Mori D, Oma Y, Takeshita Y, Sasagawa N, Ishiura S. Muscleblind protein, MBNL1/EXP, binds specifically to CHHG repeats. Hum Mol Genet 2004;13:495–507.

[11] Kanadia RN, Johnstone KA, Mankodi A, Lungu C, Thornton CA, Esson D, et al. A muscleblind knockout model for myotonic dystrophy. Science 2003;302:1978–80.

[12] Ho TH, Charlet-B N, Poulos MG, Singh G, Swanson MS, Cooper TA. Muscleblind proteins regulate alternative splicing. EMBO J 2004;74:1309–13.

[13] Dansithong W, Paul S, Comai L, Reddy S. MBNL1 is the primary determinant of focus formation and aberrant insulin receptor splicing in DM1. J Biol Chem 2005;280:5773–80.

[14] Savkur RS, Philips AV, Cooper TA. Aberrant regulation of insulin receptor alternative splicing is associated with insulin resistance in myotonic dystrophy. Nat Genet 2001;29:40–7.

[15] Charlet-B N, Savkur RS, Singh G, Philips AV, Grice EA, Cooper TA. Loss of the muscle-specific chloride channel in type 1 myotonic dystrophy due to misregulated alternative splicing Mol. Cell 2002;10:45–53.

[16] Zhang W, Liu H, Han K, Grabowski PJ. Region-specific alternative splicing in the nervous system: implications for regulation by the RNA-binding protein NAPOR. RNA 2002;8: 671–85.

[17] Gromak N, Matlin AJ, Cooper TA, Smith CW. Antagonistic regulation of alpha-actinin alternative splicing by CELF proteins and polypyrimidine tract binding protein. RNA 2003;9:443–56.

[18] Faustino NA, Cooper TA. Identification of putative new splicing targets for ETR-3 using sequences identified by systematic evolution of ligands by exponential enrichment. Mol Cell Biol 2005;25:879–87.

[19] Ladd AN, Charlet N, Cooper TA. TheCELF family of RNA binding proteins is implicated in cell-specific and developmentally regulated alternative splicing. Mol Cell Biol 2001;21: 1285–96.

[20] Timchenko NA, Welm AL, Lu X, Timchenko LT. CUG repeat binding protein (CUGBP1) interacts with the 5′ region of C/EBPbeta mRNA and regulates translation of C/EBPbeta isoforms. Nucleic Acids Res 1999;27:4517–25.

[21] Good PJ, Chen Q, Warner SJ, Herring DC. A family of human RNA-binding proteins related to the Drosophila Bruno translational regulator. J Biol Chem 2000;275:28583–93.

[22] Paillard L, Legagneux V, Beverley Osborne H. A functional deadenylation assay identifies human CUG-BP as a deadenylation factor. Biol Cell 2003;95:107–13.

[23] Timchenko NA, Patel R, Iakova P, Cai ZJ, Quan L, Timchenko LT. Overexpression of CUG triplet repeat-binding protein, CUGBP1, in mice inhibits myogenesis. J Biol Chem 2004;279: 13129–39.

[24] Ho TH, Bundman D, Armstrong DL, Cooper TA. Transgenic mice expressing CUG-BP1 reproduce splicing mis-regulation observed in myotonic dystrophy. Hum Mol Genet 2005;14: 1539–47.

[25] Cooper TA, Ordahl CP. A single cardiac troponin T gene generates embryonic and adult isoforms via developmentally regulated alternate splicing. J Biol Chem 1985;260:11140–8.
[26] Cooper TA. Muscle-specific splicing of a heterologous exon mediated by a single muscle-specific splicing enhancer from the cardiac troponin T gene. Mol Cell Biol 1998;18:4519–25.
[27] Savkur RS, Philips AV, Cooper TA. Aberrant regulation of insulin receptor alternative splicing is associated with insulin resistance in myotonic dystrophy. Nat Genet 2001;29:40–7.
[28] Charlet-B N, Savkur RS, Singh G, Philips AV, Grice EA, Cooper TA. Loss of the muscle-specific chloride channel in type 1 myotonic dystrophy due to misregulated alternative splicing. Mol Cell 2002;10:45–53.
[29] Timchenko NA, Cai ZJ, Welm AL, Reddy S, Ashizawa T, Timchenko LT. RNA CUG repeats sequester CUGBP1 and alter protein levels and activity of CUGBP1. J Biol Chem 2001;276: 7820–6.
[30] Roberts R, Timchenko NA, Miller JW, Reddy S, Caskey CT, Swanson MS, et al. Altered phosphorylation and intracellular distribution of a (CUG)n triplet repeat RNA-binding protein in patients with myotonic dystrophy and in myotonin protein kinase knockout mice. Proc Natl Acad Sci USA 1997;94:13221–6.
[31] Malinina L. Possible involvement of the RNAi pathway in trinucleotide repeat expansion diseases. J Biomol Struct Dyn 2005;23:233–5.
[32] Philips AV, Timchenko LT, Cooper TA. Disruption of splicing regulated by a CUG-binding protein in myotonic dystrophy. Science 1998;280:696–7.
[33] Kanadia RN, Urbinati CR, Crusselle VJ, Luo D, Lee YJ, Harrison JK, et al. Developmental expression of mouse muscleblind genes Mbnl1, Mbnl2 and Mbnl3. Gene Expr Patterns 2003;3:459–62.
[34] Ladd AN, Charlet N, Cooper TA. The CELF family of RNA binding proteins is implicated in cell-specific and developmentally regulated alternative splicing. Mol Cell Biol 2001;21: 1285–96.
[35] Ladd AN, Stenberg MG, Swanson MS, Cooper TA. Dynamic balance between activation and repression regulates pre-mRNA alternative splicing during heart development. Dev Dyn 2005;233:783–93.

Human Molecular Genetics, 2007, Vol. 16, No. 2 *115–128*
doi:10.1093/hmg/ddl446
Advance Access published on December 12, 2006

A *Gne* knockout mouse expressing human V572L mutation develops features similar to distal myopathy with rimmed vacuoles or hereditary inclusion body myopathy

May Christine V. Malicdan, Satoru Noguchi*, Ikuya Nonaka, Yukiko K. Hayashi and Ichizo Nishino

Department of Neuromuscular Research, National Institute of Neuroscience, National Center of Neurology and Psychiatry, 4-1-1 Ogawahigashi-cho, Kodaira, Tokyo 187-8502, Japan

Received October 3, 2006; Revised November 2, 2006; Accepted November 21, 2006

Distal myopathy with rimmed vacuoles (DMRV) or hereditary inclusion myopathy (h-IBM) is an early adult-onset distal myopathy caused by mutations in the UDP-*N*-acetylglucosamine 2-epimerase/ *N*-acetylmannosamine kinase (*GNE*) gene which encodes for a bifunctional enzyme involved in sialic acid biosynthesis. It is pathologically characterized by the presence of rimmed vacuoles especially in atrophic fibers, which also occasionally contain congophilic materials that are immunoreactive to β-amyloid, lysosomal proteins, ubiquitin and tau proteins. To elucidate the pathomechanism of this myopathy and to explore the treatment options, we generated a mouse model of DMRV/h-IBM. We knocked out the *Gne* gene in the mouse, but this resulted in embryonic lethality. We therefore generated a transgenic mouse that expressed the human *GNE*V572L mutation, which is the most prevalent among Japanese DMRV patients, and crossed this with $Gne^{(+/-)}$ mouse to obtain $Gne^{(-/-)}$h*GNE*V572L-Tg. Interestingly, these mice exhibit marked hyposialylation in serum, muscle and other organs. Reduction in motor performance in these mice can only be seen from 30 weeks of age. A compelling finding is the development of β-amyloid deposition in myofibers by 32 weeks, which clearly precedes rimmed vacuole formation at 42 weeks. These results show that the $Gne^{(-/-)}$ h*GNE*V572L-Tg mouse mimics the clinical, histopathological and biochemical features of DMRV/h-IBM, making it useful for understanding the pathomechanism of this myopathy and for employing different strategies for therapy. Our findings underscore the notion that hyposialylation plays an important role in the pathomechanism of DMRV/h-IBM.

INTRODUCTION

Distal myopathy with rimmed vacuoles (DMRV) is an autosomal recessive myopathy which was originally reported by Nonaka *et al.*, (1) thus it is also known as Nonaka myopathy. It is the same entity with hereditary inclusion body myopathy (h-IBM), which was initially reported among Iranian Jews (2). DMRV/ h-IBM usually starts affecting adults from ages 15 to 40 years with an average onset of 26 years and with an initial symptom of altered gait (1). It is gradually progressive, and patients become wheelchair-bound between 26 and 57 years of age, or about an average of 12 years after the onset of symptoms (3).

DMRV/h-IBM is characterized by preferential involvement of the distal muscles of lower extremities especially the tibialis anterior muscles, with relative sparing of the quadriceps, hence the term 'quadriceps-sparing' rimmed vacuolar myopathy (2). Other muscles are involved as well, especially late in the course of the disease (3). Serum creatine kinase (CK) level is normal or mildly elevated. The characteristic finding on muscle biopsy is the presence of rimmed vacuoles (RVs), which are actually empty spaces surrounded by aggregation of autophagic vacuoles. These RVs occasionally contain congophilic materials that are immunoreactive to various proteins, including amyloid β, phosphorylated tau, ubiquitin and

*To whom correspondence should be addressed. Tel: +81 423461712; Fax: +81 423461742; Email: noguchi@ncnp.go.jp

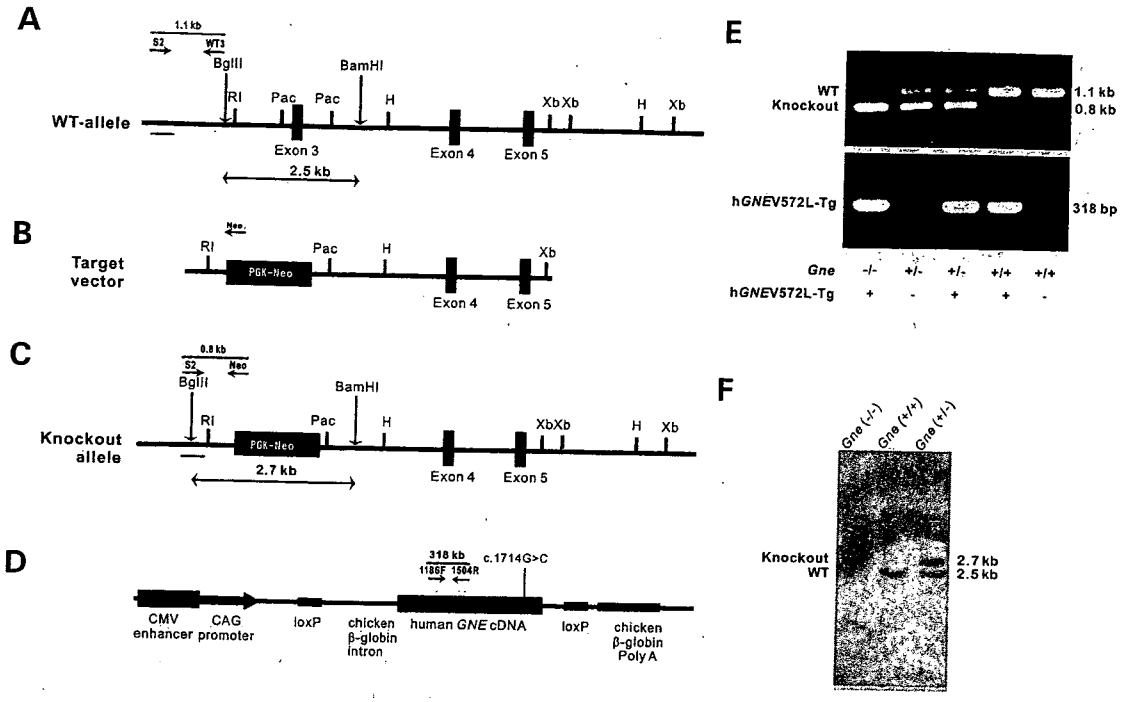

Figure 1. Genomic configuration of the *Gne* gene and targeting vector. Schematic structure of the WT *Gne* gene (**A**), which contains exon 3–5. Positions of restriction enzyme sites are shown. H, *Hin*dIII; Pac, *Pac*I; RI, *Eco*RI; Xb, *Xba*I. A 10.5 kb *Eco*RI–*Xba*I fragment was subcloned to make the targeting vector (**B**). One side of the Neo cassette was inserted 1.4 kb upstream of exon 3, and the other side of which was inserted 124 bp downstream of exon 3. In the knockout allele (**C**), the Neo cassette replaced the 1.4 kb upstream of exon 3, exon 3 and 124 bp downstream of exon 3. We selected homologous recombinants by neomycin resistance. (**D**) Structure of mutated human *GNE*V572L construct. CAG promoter was used to achieve expression in various tissues. (**E**) Genotyping of *Gne* and h*GNE*V572L-Tg mice by PCR. Five genotypes resulting from crossing a $Gne^{(+/-)}$h*GNE*V572L-Tg and $Gne^{(+/-)}$ are shown [from left to right: $Gne^{(-/-)}$ h*GNE*V572L-Tg (+); $Gne^{(+/-)}$h*GNE*V572L-Tg(−); $Gne^{(+/-)}$h*GNE*V572L-Tg(−); $Gne^{(+/+)}$h*GNE*V572L-Tg(+); and $Gne^{(+/+)}$h*GNE*V572L-Tg(−)]. In *Gne* genotyping (upper panel), the 0.8 and 1.1 kb bands represent knockout and WT alleles, respectively [PCR products amplified by primer sets are illustrated in (A) and (C)]. In h*GNE*V572L-Tg genotyping (lower panel), the presence of 318 bp band represents the integration of the h*GNE*V572L transgene. (**F**) Confirmation of *Gne* genotypes by Southern blot analysis. Tail genomic DNA were digested with *Bgl*II and *Bam*HI and analyzed by Southern blot analyses with 5′ probes shown as bars in (A) and (C). The fragments of 2.7 and 2.5 kb represent knockout and WT alleles, respectively.

α-synuclein. Necrotic and regenerating fibers and areas of inflammation are uncommon but can be seen. Ultrastructurally, filamentous inclusions measuring 18–20 nm in diameter are seen in both the cytoplasm and nucleus (3), in addition to the presence of autophagy and various inclusions.

DMRV/h-IBM was mapped to chromosome 9 (4,5), and was shown to be associated with mutations in the *GNE* gene (6,7), which encodes for a bifunctional enzyme that catalyzes the rate-limiting step in sialic acid biosynthesis (8). All patients acquire the disease by autosomal recessive pattern, and have at least one missense mutation in one allele, including the most common mutations V572L and M712T among Japanese and Iranian Jews, respectively. No patient with homozygous null mutation was identified. Genetically confirmed DMRV/h-IBM diseases, initially recognized among Japanese and Iranian Jews (6,9–11), appear to afflict patients with diverse nationalities and cultural backgrounds (12–16).

The mechanism by which mutations in the *GNE* lead to the phenotype in DMRV/h-IBM has remained unclear. We previously demonstrated that mutations in the *GNE* led to the reduction in either the UDP-GlcNAc 2-epimerase or ManNAc kinase activity (17); moreover, we have shown that myotubes from DMRV patients are hyposialylated, and this phenomenon can be corrected by the addition of free sialic acid and/or its precursor. Other groups have shown similar results regarding GNE activity, but in contrast, they suggested that only the cells derived from a patient carrying a homozygous epimerase mutation had a significant reduction in the overall membrane-bound sialic acid (18), and that *GNE* mutations may not contribute to alteration in sialylation in h-IBM myoblasts (19). To address these issues, we developed a mouse model for the disease. In this article, we present the first DMRV/h-IBM mouse model that expressed only the mutated human *GNE* and show that this mouse evidently displays features of DMRV/h-IBM seen in human patients.

RESULTS

Production of $Gne^{(-/-)}$h*GNE*V572L-Tg

In Figure 1, the genomic configuration of the *Gne* gene (A) and the targeting construct (B) are shown. The inserted Neo cassette replaced the 1.4 kb upstream of exon 3, exon 3 and 1.4 kb downstream of exon 3. Only WT and $Gne^{(+/-)}$ mice were generated; no $Gne^{(-/-)}$ mouse was produced (data not shown), in concurrence with a previous report (20). We then proceeded to generate a transgenic mouse (h*GNE*V572L-Tg) that expressed the human mutated *GNE* with V572L, the most common *GNE* mutation in Japan, the structure of which is shown in Figure 1D. Of the resulting litters, nine

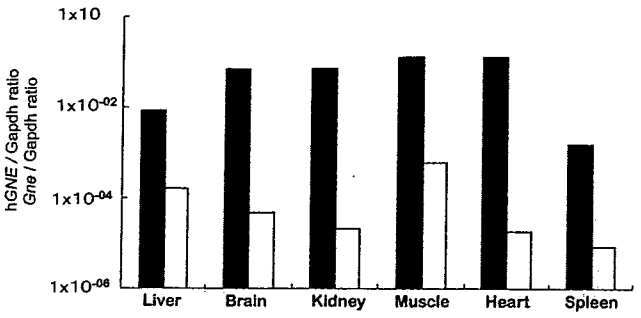

Figure 2. Expression of h*GNE*V572L (closed bars) and endogenous *Gne* (open bars) relative to Gapdh. Log-values were used for computation of ratio. Highest expression of h*GNE*V572L is seen in skeletal and cardiac muscles, followed by heart, kidney, brain, liver and spleen.

mice were found to incorporate the h*GNE*V572L by PCR analysis of genomic DNA isolated from tail snips, but only four lines were able to generate offspring. Using quantitative RT-PCR, we quantified mRNA expression of h*GNE*V572L and endogenous *Gne* in muscle and other organs of these transgenic mice. Transgene expression was highest in the skeletal muscle, followed by heart, kidney, brain, spleen and liver (Fig. 2), while endogenous *Gne* expression was barely detected. We also determined the copy number using quantitative PCR by comparing the amplification of h*GNE*V572L with endogenous *Gne*. We calculated the copy numbers for lines 3, 6, 7 and 9 as 2, 4, 3 and 5, respectively. Consequently, we used this transgenic line 9 for producing the model mouse.

We crossed the h*GNE*V572L transgenic mouse with a $Gne^{(+/-)}$ to obtain a $Gne^{(+/-)}$h*GNE*V572L-Tg. Further, we crossed this $Gne^{(+/-)}$h*GNE*V572L-Tg with a $Gne^{(+/-)}$ to generate our model mouse, a transgenic mouse on a *Gne* knockout background, $Gne^{(-/-)}$h*GNE*V572L-Tg. Analysis of 823 newborn mice from independent heterozygous crosses indicated that the numbers of mice with the five genotypes, $Gne^{(-/-)}$h*GNE*V572L-Tg (+), $Gne^{(+/-)}$h*GNE*V572L-Tg(+), $Gne^{(+/-)}$h*GNE*V572L-Tg(−), $Gne^{(+/+)}$h*GNE*V572L-Tg(+) and $Gne^{(+/+)}$h*GNE*V572L-Tg(−) were 72 (9%), 225 (28%), 193 (24%), 177 (22%) and 136 (17%), respectively, almost approximating the expected ratio of Mendelian inheritance. Mice of the latter four genotypes did not demonstrate unusual phenotype, and thus were considered as control littermates. Images for routine PCR for checking *Gne* genotype and the incorporation of the human *GNE*V572L are shown in Figure 1E, with the corresponding PCR fragments illustrated in A, C and D.

Hyposialylation is evident in the $Gne^{(-/-)}$h*GNE*V572L-Tg

Understandably, mutations in the *GNE* can affect sialylation of glycoconjugates because of the gene's role in sialic acid synthesis. We therefore measured the sialic acid levels in the $Gne^{(-/-)}$h*GNE*V572L-Tg mice using HPLC with fluorometric detection. In wild-type (WT) mice, sialic acid levels are highest in the brain, followed by the liver, spleen and kidney (Fig. 3B, open boxes). In both skeletal and cardiac muscles, sialic acid levels are evidently lower than in other tissues. As we have expected, the total sialic acid in the $Gne^{(-/-)}$h*GNE*V572L-Tg mice is remarkably lower than WT. This hyposialylation is most remarkable in the serum (Fig. 3A). A significant reduction in total sialic acid level is seen in various tissues examined (Fig. 3B, closed boxes). We also measured sialic acid level in the h*GNE*V572L-Tg and noted that sialic acid levels are comparable with WT mice (Fig. 3B, gray boxes), although the transgenic expression was extremely higher than endogenous *GNE*.

$Gne^{(-/-)}$h*GNE*V572L-Tg has lower median of survival than littermate

The $Gne^{(-/-)}$h*GNE*V572L-Tg mice were indistinguishable from their littermates at birth and seemed healthy (Fig. 4A and B). After 30 weeks of age, these mice weighed less than their littermates (Fig. 4). Significant difference in weight is more pronounced and earlier in female $Gne^{(-/-)}$ h*GNE*V572L-Tg (Fig. 4C) mice when compared with male (Fig. 4D). To investigate plausible explanations for this difference in weight, we performed gross inspection of the muscles, and found out that some muscles, especially the gastrocnemius, were atrophic in the $Gne^{(-/-)}$h*GNE*V572L-Tg when compared with control (Fig. 4E and F), and this finding was more remarkable among females (Fig. 4E).

Surprisingly, the median survival rate were lower in the $Gne^{(-/-)}$h*GNE*V572L-Tg as seen in Figure 4B. The cause of death could not be ascertained, but upon necropsy, no external gross abnormalities were seen and the internal organs appeared normal. On pathological examination, five out of 12 (41%) mice that died had RVs in the skeletal muscle; among these five mice, only one was before 40 weeks of age. Twenty five percent had fibrosis and a few RVs in the diaphragm. Thirty-three percent had fibrosis in the cardiac muscles.

$Gne^{(-/-)}$h*GNE*V572l-Tg shows clinical phenotype

Using a tool for assessing general muscle strength, these mice notably performed worse than their littermates (Fig. 5A). Interestingly, significant change in muscle power is noted after 30 weeks of age. We then proceeded to measure serum CK activity in the mice and found out that CK was significantly elevated in the $Gne^{(-/-)}$h*GNE*V572L-Tg mice when compared with their littermates (Fig. 5B), albeit the observation that these values are much lower when compared with muscular dystrophy models like $Large^{myd}$ and $Sgcb^{(-/-)}$ mice (data not shown). Because the appearance of phenotype seemed to be related to age, we measured CK activity according to different age groups. From Figure 5C, we note that elevation of CK activity starts at 30 weeks of age. Using gel electrophoresis, we verified that CK-MM isozyme was primarily increased (data not shown).

$Gne^{(-/-)}$h*GNE*V572l-Tg shows characteristic pathological features of DMRV

We checked if the $Gne^{(-/-)}$h*GNE*V572L-Tg mice showed muscle phenotype not only by the analysis of muscle power

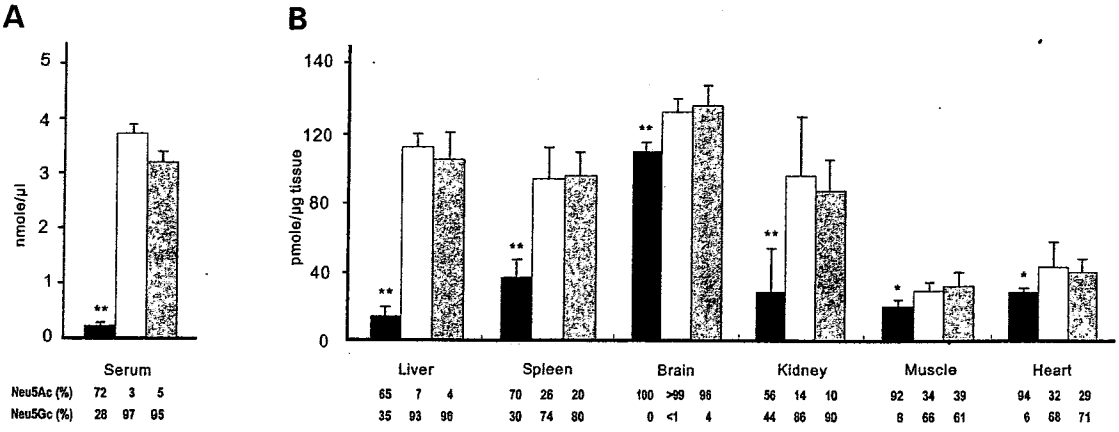

Figure 3. Measurement of total sialic acid in serum (**A**) and tissues (**B**) in *Gne*$^{(-/-)}$h*GNE*V572L-Tg (closed bars), WT (open bars) and h*GNE*V572L-Tg (gray bars); bars represent mean total sialic acid level with SD. Breakdown of sialic acid contents according to standards used (Neu5Ac and Neu5Gc) are shown below. Sialic acid levels of WT and h*GNE*V572L-Tg are comparable. Note the reduction of sialic acid levels in the serum and tissues of the *Gne*$^{(-/-)}$h*GNE*V572L-Tg mice. Single asterisk, $P < 0.05$; double asterisks, $P < 0.005$.

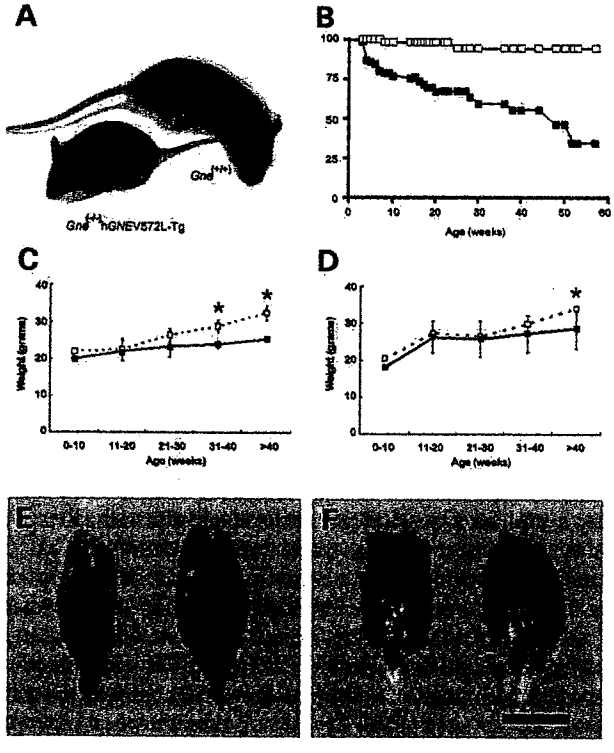

Figure 4. Overall phenotype of the *Gne*$^{(-/-)}$h*GNE*V572L-Tg mice. (**A**) Picture of WT (up) and *Gne*$^{(-/-)}$h*GNE*V572L-Tg (down) at 16 weeks of age. (**B**) Survival curve of mice: WT (open squares, $n = 71$ for males and females), *Gne*$^{(-/-)}$h*GNE*V572L-Tg mice (closed squares, $n = 71$ for males and females). *Gne*$^{(-/-)}$h*GNE*V572L-Tg mice have significantly reduced life spans when compared with WT mice (log-rank test: $P = 0.001$). (**C**) Growth curves of female: WT (open squares, $n = 10$ per age group), *Gne*$^{(-/-)}$h*GNE*V572L-Tg mice (closed squares, $n = 10$ per age group) (**D**) Growth curves of male mice: WT (open squares, $n = 10$ per age group), *Gne*$^{(-/-)}$h*GNE*V572L-Tg (closed squares, $n = 10$ per age group). *Gne*$^{(-/-)}$h*GNE*V572L-Tg mice have lower body weight after 30 weeks of age, and this is more pronounced in females; asterisk denotes $P < 0.05$, Mann–Whitney U test. Gastrocnemius muscles of female (**E**) and male (**F**) mice: *Gne*$^{(-/-)}$h*GNE*V572L-Tg (left) and littermate (right). Atrophy is noted on gross inspection of h*GNE*V572L-Tg gastrocnemius muscles; bar represents 5 mm.

but also by evaluating biopsy samples in five different age groups (10, 20, 30, 40 and 50 weeks). Morphometric analysis of the fibers in different age groups showed that the variation in fiber size becomes more marked with age, preferentially affecting the gastrocnemius and quadriceps muscles (data not shown); for this reason, we used the gastrocnemius muscle in further experiments. We found that at young age, they developed neither clinical nor pathological phenotype, as they were comparable with WT. Figure 6A, D and G shows representative sections from the *Gne*$^{(-/-)}$ h*GNE*V572L-Tg mice per age group. Histopathological analysis revealed almost normal findings in the muscle sections before 30 weeks of age (data not shown). In general, necrotic and regenerating processes are not observed in the young mice, although a few necrotic fibers are observed as they grow older. No endomysial or perimysial inflammation is seen.

Scattered small angular fibers are noted by 30 weeks of age (Fig. 6A), which is not seen in the littermates (Fig. 6B and C). The variation in fiber size becomes more noticeable as the mice grow older. In addition, fibers appear atrophic by 40 weeks of age, in support with the observation that the gastrocnemius muscle is relatively atrophic by gross inspection. Remarkably after 40 weeks, RVs are seen in scattered fibers (arrows in Fig. 6D and G). Occasionally, inclusion bodies are found in the fibers with or without RVs (arrowhead in Fig. 7A and B). Like in humans, these RVs are intensely stained with acid phosphatase, giving the impression that autophagic process is activated (Fig. 7C). We confirmed this by checking the expression of lysosomal-associated proteins (LAMPs) 1 and 2, and LC3 in muscle sections, all of which are upregulated. LAMP-1 is predominantly expressed within the vicinity of RVs (Fig. 7E). LAMP-2, on the other hand, noticeably is also expressed in the subsarcolemmal areas aside from its localization in the area of RVs (Fig. 7F). LC3 immunoreactivity is almost similar to LAMP-2, except that the perinuclear region is also highlighted (Fig. 7G).

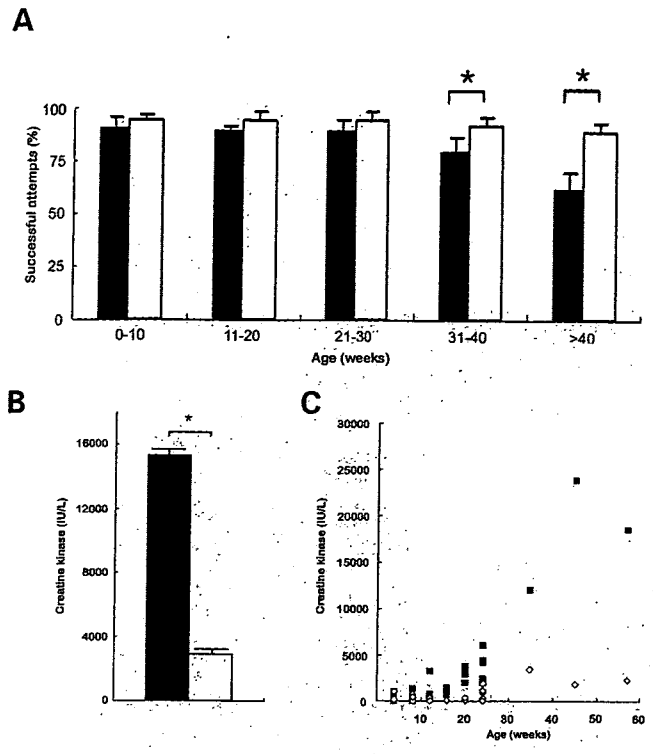

Figure 5. (A) Evaluation of over-all motor strength using rod-climbing test, according to age group. Mean of three trials are shown. $Gne^{(-/-)}$ h*GNE*V572L-Tg mice (closed bars, $n = 10$) perform worse than littermates ($n = 10$). Significant difference is noticeable after 30 weeks of age. Asterisk, $P < 0.05$ (Mann–Whitney U test). (B) Measurement of CK activity. Serum CK is significantly higher in $Gne^{(-/-)}$h*GNE*V572L-Tg mice (closed bars) when compared with littermates (open bars). Asterisk, $P < 0.05$ (Student's t-test, two-tailed). (C) CK activity according to age. CK activity of $Gne^{(-/-)}$ h*GNE*V572L-Tg mice (closed squares) starts to elevate after 30 weeks of age when compared with littermates (open diamonds).

Various proteins are expressed in the $Gne^{(-/-)}$h*GNE*V572L-Tg muscles

One of the defining hallmark features of DMRV/h-IBM is the presence of inclusion bodies that are presumed to have a role in muscle degeneration. These deposits have been shown to be immunoreactive to several proteins. Similar to human cases of DMRV, muscle cross sections obtained from the $Gne^{(-/-)}$ h*GNE*V572L-Tg mice reveal positive Congo red staining (Fig. 7D), which is not observed in the myofibers of control mice (data not shown). Intense, demarcated signals are seen within the area of RVs and more frequently co-localizing with inclusion bodies which are often seen in DMRV/h-IBM. As congophilia denotes deposition of proteins assuming a beta-pleated structure, we used the well-characterized 6E10, Aβ1–42, Aβ1–40 and A11 (amyloid β-oligomer), and β-site amyloid precursor protein cleaving enzyme (BACE2) antibodies to check for intracellular accumulation of amyloid. Amyloid depositions occur within the myofibers, and are seen to be occasionally associated with vacuolated fibers, as ~62% of RVs are positive for amyloid expression (data not shown). These amyloid inclusions are also noted in non-vacuolated fibers, including those which appear normal. Amyloid β precursor protein (AβPP), which is recognized by 6E10 antibody (Fig. 7I) has intense, large, fairly demarcated immunoreactive signals within the RVs, similar to the staining pattern of the fibrillar forms of amyloid β or amyloid β peptides 1–42 and 1–40 (Fig. 7J and K). In good agreement with finding amyloid deposits in the myofibers, BACE2, which purportedly represents β-secretase activity, is upregulated in these myofibers and are seen as granular staining in the cytoplasm and intense immunoreactivity at subsarcolemmal areas (Fig. 7H). Interestingly, the oligomer form of amyloid β, which is recognized by A11, is also expressed in the myofibers; positive signals are seen as aggregates around the RVs which are localized in areas distinct from fibrillar forms of amyloid (Fig. 7L).

We then analyzed skeletal muscles of mice from different age groups to see whether these amyloid accumulations are related to or can be considered as a function of age. We found out that these accumulations start to occur from 32 to 34 weeks of age, a period when virtually no RV is seen in the myofibers, and muscle pathology is characterized mainly by mild variation in fiber size (Fig. 8A and C). Both AβPP (Fig. 8B) and amyloid β 1–42 peptide (Fig. 8D) show positive immunoreactivity within the myofibers.

The microtubule-associated protein tau, a cytoskeletal protein, has been shown to be abnormally phosphorylated and accumulated in DMRV and other muscle disorders (21–23). Similarly, in these mice, these deposits are evident as squiggly inclusions which are occasionally seen in vacuolated fibers (Fig. 7M).

SM-31, an antibody which detects neurofilaments, has been well-characterized in DMRV/h-IBM (21,24). In muscle sections, positive staining is seen within the vicinity of RVs (Fig. 7N); not all RVs, however, show immunoreactivity with this antibody. SM-310, on the other hand, only stains the intramuscular nerve bundles (Fig. 7O).

Because of the accumulation of several proteins in the myofibers, ER stress and the unfolded protein response (UPR) have been implicated in the pathogenesis of DMRV/h-IBM. Using an antibody which recognizes one of the ER chaperones, we show that the UPR activation occurs in the $Gne^{(-/-)}$ h*GNE*V572L-Tg mice. Intracellular Grp-94 immunoreactivity is seen exclusively in vacuolated fibers (Fig. 7P). In the myofibers of the mice, strong reactivity to ubiquitin antibody in vacuolated and non-vacuolated fibers are seen (Fig. 7Q), suggesting that the ubiquitin–proteosome system may as well be involved in the degradation of abnormal protein accumulations in the muscle, and that misfolded proteins are ubiquitinated but not degraded.

Sarcolemmal proteins are also accumulated in DMRV/h-IBM myofibers. Within the vicinity of the RVs, positive α-dystroglycan (Fig. 7R), β-dystroglycan (Fig. 7S) and α-sarcoglycan (Fig. 7T) signals are observed.

In the myofibers of the control mice, no protein depositions were appreciated (data not shown).

Electron microscopic studies show evidence of autophagy and inclusions in the $Gne^{(-/-)}$h*GNE*V572L-Tg muscles

Ultrastructural studies confirm the activation of autophagy in $Gne^{(-/-)}$h*GNE*V572L-Tg muscles (Fig. 9). We obtained samples from a 42-week-old female mouse which had RVs

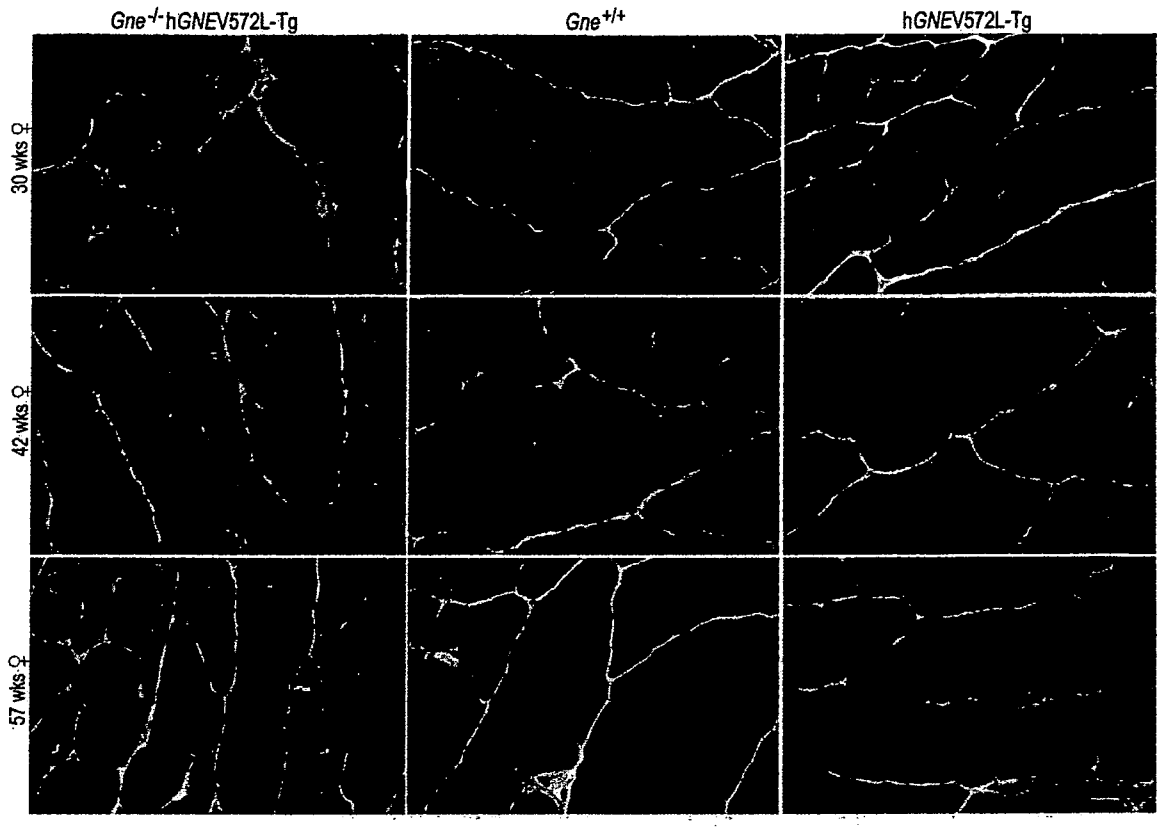

Figure 6. Hematoxylin and eosin sections from *Gne*$^{(-/-)}$h*GNE*V572L-Tg (**A, D, G**), WT (**B, E, H**), h*GNE*V572L-Tg (**C, F, I**). The h*GNE*V572L-Tg mice are comparable with WT in all ages. In the *Gne*$^{(-/-)}$h*GNE*V572L-Tg, there is variation in fiber size which becomes more obvious as the mice age. Fibrosis, necrotic or regenerating processes are not noted. Internalized nuclei are noted in scattered fibers. Small angular fibers are noted from around 30 weeks of age (A, arrows). Fibers with RVs (arrows), as well as cytoplasmic inclusions (arrowhead) are observed in scattered fibers from 42 weeks of age (D and G). Bar represents 40 μm.

as seen in light microscopy. In these samples, disorganization of myofibrils was seen in the vicinity of RVs. In about 500 myofibers examined, 10% showed ultrastructural evidence of autophagy. Collections of lysosomal autophagosomes containing undigested intracellular debris were seen, usually enclosed by a limiting membrane (Fig. 9A, arrow). The debris are often composed of light or electron-dense amorphous materials, and appeared like myelin whorls. Multiple small double membrane-bound autophagic vacuoles were often contained within a larger autophagic vesicle (AV), suggesting that autophagy in these myofibers involves a continual process of AV consolidation (Fig. 9A, arrowhead). Multilamellar bodies are also observed (Fig. 9A, double arrows). Probable amyloid deposits are seen as amorphous and granular material (Fig. 9B, magnified from A). Interestingly, ovoid and densely granular deposits, which may also be amyloid-like structures, are noted not only in the areas of autophagy (Fig. 9A, asterisk), but also in areas where myofibrillar architecture is well preserved (Fig. 9C). Occasionally, autophagic vacuoles are seen within the substance of these deposits (Fig. 9C, arrow).

Gne$^{(-/-)}$h*GNE*V572L-Tg shows pathological changes in the diaphragm and cardiac muscles

It has been a well-accepted fact that DMRV/h-IBM primarily involved the skeletal muscles, and that respiratory muscles are assumed to be spared as there had been no reports implying the involvement of the respiratory system. Interestingly, in the *Gne*$^{(-/-)}$h*GNE*V572L-Tg mice, we found that even diaphragm muscles are involved, although the findings range from almost normal findings to the presence of marked fibrosis and RVs in the myofibers (Fig. 10A). Likewise, we have observed inclusion bodies which are seen in both vacuolated and non-vacuolated fibers (data not shown).

It is now being recognized that some patients manifest with a variety of cardiac abnormalities, from the seemingly benign right bundle branch block to fatal arrhythmias. This led us to carefully check the status of cardiac muscles in the mice. We found out that few mice (around 20%) develop fibrosis in the cardiac tissue after the age of 30 weeks, and some show marked endomysial fibrosis (Fig. 10B). Moreover, amyloid deposition (Fig. 10C) and, occasionally, RVs (Fig. 10D) are also observed in cardiomyocytes. We also tried to functionally evaluate the heart using 2D echocardiography and electrocardiogram, but we did not observe any abnormality pointing to definite cardiomyopathy or conduction defects (data not shown), although we only tested a limited number of mice.

DISCUSSION

Sialylation of oligosaccharide chains is a common and physiologically important event, and sialic acids are probably the

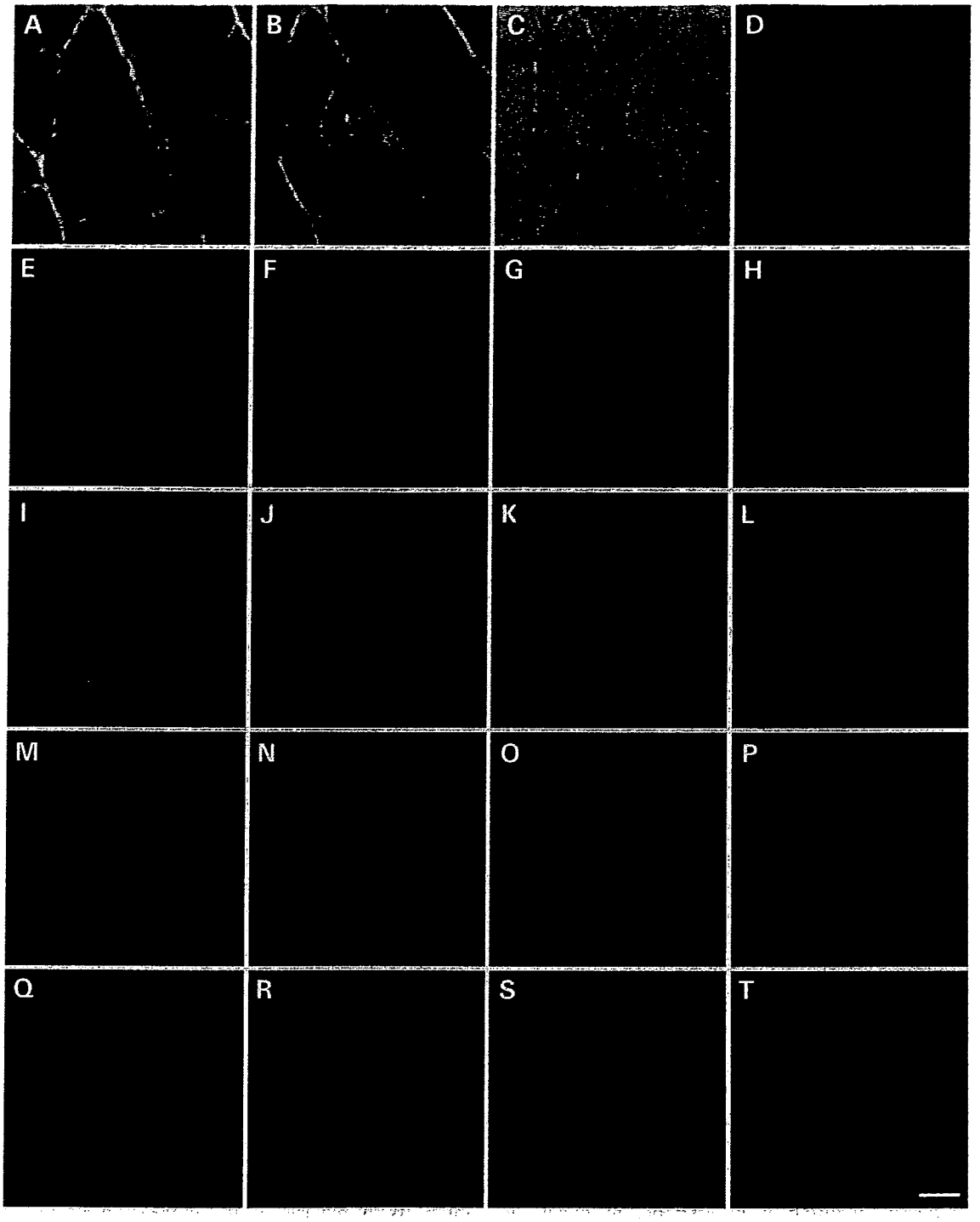

Figure 7. Serial sections taken from a 42-week-old female *Gne*$^{(-/-)}$h*GNE*V572L-Tg mouse. (**A**) Hematoxylin and eosin sections show fibers with RVs and cytoplasmic inclusions. (**B**) In modified Gomori trichrome, vacuoles are rimmed by eosinophilic granules. (**C**) Acid phosphatase activity is enhanced around RVs, suggesting upregulation of lysosomal activity in these areas. (**D**) Congo red staining visualized by Texas red filters shows positive staining in fibers with or without RVs, and appear as large, granular deposits. Immunoreactivity to lysosomal proteins confirm the presence of autophagy in fibers with RVs: (**E**) LAMP-1 signals are seen in the areas of RVs; (**F**) LAMP-2 has subsarcolemmal immunoreactivity, in addition to positive staining in RVs; (**G**) LC3 stains the same areas as LAMP-2, in addition to the perinuclear areas. Intracellular deposition of amyloid is seen in vacuolated or non-vacuolated fibers: (**H**) Increased reactivity to BACE2 is seen in the cytoplasm of fibers with RVs and within the vicinity of RVs; (**I**) AβPP expression is intense in area of RVs, seen as discrete deposits; (**J**) amyloid β 1–42 and (**K**) amyloid β 1–40 stainings are likewise seen as discrete deposits within the vicinity of RVs; (**L**) amyloid β-oligomeric antibody signals are noted as aggregates of small granule-like deposits around the RVs. Neurofilament deposition is observed in the myofibers: SM-31 (**M**) immunoreactivity is occasionally noted within the vicinity of RVs, whereas SM-310 (**N**) only stains intramuscular nerve bundles. (**O**) Epitopes of phosphorylated tau are observed in some fibers with RVs. (**P**) Fibers with RVs have intense ubiquitin staining around RVs and granule-like signals in these fibers. (**Q**) Grp94, an endoplastic reticulum luminal stress protein, is upregulated exclusively in vacuolated fibers as large granular deposits within the RVs. Sarcolemmal proteins are deposited within the vicinity of RVs: (**R**) α-dystroglycan; (**S**) β-dystroglycan; and (**T**) α-sarcoglycan. Bar represents 20 μm.

Figure 8. Ultrastructural evidence of autophagy and intracellular inclusions. (**A**) Collections of lysosomal autophagosomes with intracellular debris which are light or electron-dense amorphous materials enclosed by a limiting membrane (arrow). Multilammelar structures are also observed (double arrows). Ovoid and dense deposits which are probably amyloid deposits are likewise seen (asterisk). (**B**) Probable amyloid deposits are seen as amorphous and granular material surrounded by autophagosomes (B: magnified from A). (**C**) Dense, granular deposits which are probably amyloid accumulations are also noted in areas where architecture of myofibrils are generally well-preserved; occasionally, autophagic vacuoles are seen within the substance of these deposits (arrow). Bar represents 2 μm.

most biologically important monosaccharide units of glycoconjugates. These negatively charged sugars at the terminal ends of glycoconjugates have very important biological roles in mammalian development, and this is underscored by the embryonic lethality resulting from attempts to knock-out *Gne* in the mice (20), and further supported by the absence of homozygous null mutations in humans. Making a transgenic *GNE* mouse on a *Gne* knockout background thus allowed us to rescue the phenotype in *Gne* knockout. Clearly, the $Gne^{(-/-)}$h*GNE*V572L-Tg resembles the phenotype in human DMRV/h-IBM patients.

It is conceivable that a mutation in the *GNE*, a gene responsible for catalyzing the rate-limiting step in sialic acid biosynthesis, can lead to hyposialylation. Most, if not all, of the mutations causing DMRV caused partial reduction of the enzymatic activity of either UDP-GlcNAc 2-epimerase or ManNAc kinase of the GNE (17,19). As we have predicted, our results show that there is a marked reduction in sialic acid level, which can reflect the enzymatic activity of GNE, in the serum and other tissues of the $Gne^{(-/-)}$h*GNE*V572L-Tg mice. With regards to the expression of *GNE* in various tissues, it has been shown that expression in the muscle is very low (25). Our results show, on the other hand, that mRNA expression of h*GNE*V572L-Tg is highest in the muscle, and we attribute this to the promoter that we used in the transgene construct. Previously, we have shown that CAG promoter efficiently promotes expression of a gene into adult skeletal muscles (26).

Skeletal muscle is mainly affected in DMRV/h-IBM, although it is reasonable to expect multi-organ involvement because of the ubiquitous expression of *GNE*. In our mice, the skeletal muscle is clearly affected despite the data that

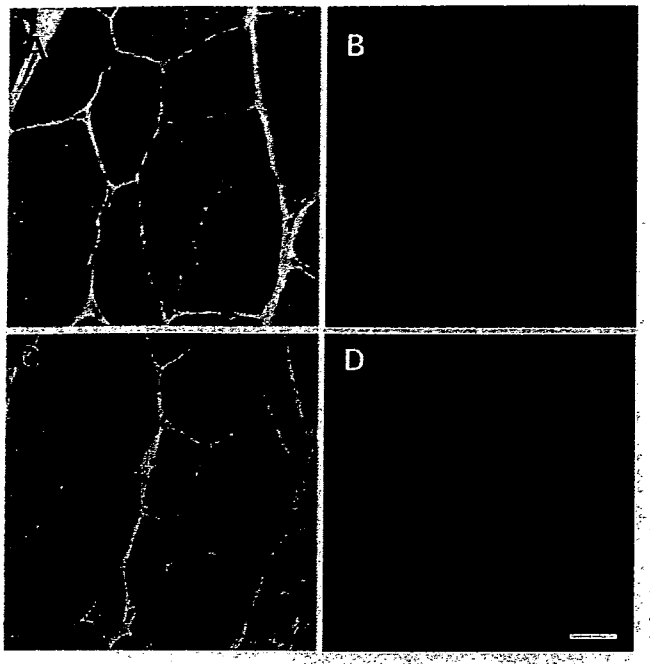

Figure 9. Amyloid deposition precedes RV formation. Sections taken from the gastrocnemius of a 34-week-old female mouse shows variation in fiber size in hematoxylin and eosin sections (**A** and **C**). Note the absence of RVs or cytoplamic inclusions in these fibers. Amyloid depositions are seen as immunofluorescent signals in small fibers (**B**, amyloid β 1–42; **D**, AβPP). Bar represents 20 μm.

hyposialylation is not that remarkable when compared with other organs. Our results suggest that even a slight reduction in sialic acid level can cause symptoms in skeletal muscles; however, the selectivity of skeletal muscle may not be explained by the *Gne* expression levels and sialic acid levels in each organ.

It is notable that some of the $Gne^{(-/-)}$h*GNE*V572L-Tg mice die sooner than their littermates, but the precise reason for this is not known at present. It is, however, evident that a significant number of the autopsied mice showed pathological findings in the diaphragm and the heart. In humans, there was a report on two siblings with the homozygous V572L mutation who died from arrhythmia (27), but there had been no reports on respiratory involvement among patients.

The onset of symptoms among DMRV patients has been reported to be from the second to the third decade (3), although there were anecdotal reports of earlier onset (28). Interestingly, in the $Gne^{(-/-)}$h*GNE*V572L-Tg mice, the onset of clinical phenotype is noted around 30 weeks of age, which can be considered to be similar to that in humans, using lifespan and ability to reproduce for points of comparison. It is peculiar that gastrocnemius and quadriceps muscles are preferentially involved in mice, while in humans, the tibialis anterior is remarkably involved while the quadriceps are affected relatively late in the course of the disease. In our recent data on the clinical presentation of DMRV, however, it is clear that the gastrocnemius can be affected more severely in some cases (28).

We tried to check fiber type involvement in these muscles, and found out that both slow and fast fibers are affected in human and mice, in terms of the presence of RVs, but fast type fibers are predominantly involved (data not shown). Sporadic IBM has some pathological similarities with DMRV; recently, it has been shown that the presence of inclusions on routine histochemistry and the pathogenic accumulation of β-amyloid protein occur in fast twitch muscles, both in a transgenic model of IBM and in IBM patients (29), implying that fast type fibers are more vulnerable to pathological changes. Further analysis is needed on this aspect to derive a more conclusive data.

CK levels are reported to be mildly or moderately elevated in patients, although there were isolated cases where the CK activity was above 1000 IU/L (11). CK elevation has always been correlated with the presence of necrotic and regenerating processes in the skeletal muscle, but which are only occasionally found in DMRV/h-IBM. Elevation of serum CK is also seen in the $Gne^{(-/-)}$h*GNE*V572L-Tg mice, although necrotic and regenerating process is barely detectable. Our data suggest that there might be other mechanisms which trigger CK release into the circulation, aside from myonecrosis. It has not been clarified if CK release into the blood stream may be induced by deglycosylation of membrane proteins, although some studies suggested that removal of sialic acids by neuraminidase treatment may influence sarcolemmal permeability (30). Further tests are clearly needed to shed some insight on the CK elevation in DMRV/h-IBM and $Gne^{(-/-)}$h*GNE*V572L-Tg mice.

A subject of poignant interest is whether RV formation, one of the hallmarks of DMRV/h-IBM, is the primary event that induces muscle fiber atrophy and loss, notwithstanding the fact that RVs are non-specific and could be seen in a multitude of myopathies. In the $Gne^{(-/-)}$h*GNE*V572L-Tg mice, weakness is clearly noted before the occurrence of RVs, implying that other factors should be responsible for the earlier onset of weakness. Consistently, we have documented that serum and other tissues are hyposialylated, and this phenomenon is not at all correlated with age, strongly suggesting that hyposialylation may play a role in the development of clinical manifestations exhibited by patients. Previous studies have implicated that sialic acid directly contributes to the negative surface potential of cells, because desialylation of rat skeletal muscle sodium channel leads to reduced sensitivity of these channels to the effects of external calcium (31). This would mean that voltage gating parameters are shifted to the point that channels required a larger depolarization in order to gate, which may suggest that the mechanism of weakness may be due to the reduced excitability of the muscle membrane as a result of sodium channel desialylation.

The hallmarks of DMRV/h-IBM include RVs that are autophagic in nature (32) and cytoplasmic inclusions in vacuolated and non-vacuolated fibers, both of which are seen in muscle sections from the $Gne^{(-/-)}$h*GNE*V572L-Tg mice. Several proteins have been shown to accumulate in DMRV myofibers (33,34), and most of which have been demonstrated to be mainly associated with amyloid because of the positive reactivity to crystal violet and Congo red, suggesting that they assume the beta-pleated sheet configuration. In general, more than 20 unrelated proteins, including β-amyloid (34), prion, tau (21) and transthyretin, can abnormally unfold and self-aggregate to form beta-pleated sheet amyloid (35). The association of these proteins with DMRV/h-IBM